Plant mutations: slaying beautiful hypotheses by surprising evidence

Sylvain Schmitt[1,2,*], Patrick Heuret[2], Valérie Troispoux[3], Mélanie Beraud[4], Jocelyn Cazal[3], Émilie Chancerel[5], Charlotte Cravero[6], Erwan Guichoux[5], Olivier Lepais[5], João Loureiro[7], William Marande[6], Olivier Martin[8], Gregoire Vincent[2], Jérôme Chave[9], Christophe Plomion[5], Thibault Leroy[10,11,+], Myriam Heuertz[5,+], Niklas Tysklind[3,+]

[1]CNRS, UMR EcoFoG (Agroparistech, Cirad, INRAE, Université des Antilles, Université de la Guyane), Campus Agronomique, 97310 Kourou, French Guiana;[2]AMAP, Univ. Montpellier, CIRAD, CNRS, INRAE, IRD, Montpellier, France;[3]INRAE, UMR EcoFoG (Agroparistech, CNRS, Cirad, Université des Antilles, Université de la Guyane);[4]Genoscope, Institut François Jacob, Commissariat à l'Energie Atomique (CEA), Université Paris-Saclay, 2 Rue Gaston Crémieux, 91057 Evry, France;[5]Univ. Bordeaux, INRAE, BIOGECO, 69 route d'Arcachon, 33612 Cestas Cedex; [6]INRAE, (CNRGV French Plant Genomic Resource Center, F-31320, Castanet Tolosan, France);[7]Centre for Functional Ecology, Associate Laboratory TERRA, Department of Life Sciences, University of Coimbra, Calçada Martim de Freitas, 3000-456, Coimbra, Portugal;[8] URFM, INRAE, 84000 Avignon, France; [9]Laboratoire Evolution et Diversité Biologique, UMR5174, CNRS, Université Paul Sabatier, IRD, Toulouse Cedex 9, France; [10]Department of Botany and Biodiversity Research, University of Vienna, Rennweg 14, A-1030 Vienna, Austria; [11] GenPhySE, INRAE, INP, ENVT, Université de Toulouse, 24 chemin de Borde-Rouge - Auzeville Tolosane, 31326 Castanet Tolosan;[*] E-mail: sylvain.m.schmitt@gmail.com;[+] T.L., M.H., and N.T. contributed equally to this work.

Main

The Weismann theory (1) states that hereditary traits are transmitted exclusively from the germline. The theory is valid in most animals (2) where germline cells are set aside early in development (1). In plants, germline segregation is generally assumed to occur late in development (3-5), which leads to several predictions on the fate of somatic mutations occurring in plant tissues: mutations have generally low frequency in plant tissues (6); mutations at high frequency have a higher chance of intergenerational transmission; branching topology of the tree dictates mutation distribution (7); and, exposure to UV radiation increases mutagenesis (8). We produced a unique plant dataset of 60 high-coverage whole-genome sequences of two tropical tree species and identified 18,274 *de novo* somatic mutations, almost all at low frequency in tissues. We demonstrate that: 1) low-frequency mutations are transmitted to the next generation; 2) mutation phylogenies deviate from the branching topology of the tree; and 3) mutation rates and mutation spectra are not demonstrably affected by differences in UV exposure. Altogether, our results suggest far more complex links between plant growth, ageing, UV exposure, and mutation rates than commonly thought.

To identify a large set of *de novo* plant somatic mutations, we resequenced 60 samples in total for two tropical tree species, *Dicorynia guianensis* (Amshoff) and *Sextonia rubra* (Mez) van der Werff (Sup. Note A), corresponding to 3 leaves per branch for a total of up to 10 branches per tree, in addition to cambium tissues from the base of the trunk for comparison (Sup. Note B). The branches were selected as growing in either low or high light exposure, getting the benefits of the maximum contrast of forests located near the equator (5°N). Ultraviolet light (UV) exposure was assessed directly at the sampling points and additionally estimated with a canopy transmittance model inferred using terrestrial and drone lidar scans for the *D. guianensis* tree (Sup. Note C). Given that the quality of the reference genomes are known to be key aspects to ensure accurate mutation detection, we used a combination of high-fidelity reads and optical maps to generate near chromosome-level assembly for two wild tropical tree species, *D. guianensis* and *S. rubra*. The two genome assemblies differ in size (550 and 991Mb) and in their genomic content for Guanine Cytosine (GC), transposable elements, and genes, with highly heterogeneous patterns along chromosomes in *D. guianensis* vs. relatively homogeneous ones in *S. rubra* (Fig. 1, Sup. Note D). These two new high-quality annotated genomes were used as a reference to detect somatic mutations.

Using a mutation detection methodology initially developed for human cancer mutations (9) and later adapted to plants (6), we identified 15,066 unique somatic mutations in *D. guianensis* and 3,208 in *S. rubra.* Only a few were found to be restricted to a single branch (5-9%, Fig 2a-b, Sup. Note E), whereas most mutations were shared by at least two branches whose nearest shared branching point was the base of the crown (43-72%), thus originating below the base of the crown. We further tested the correspondence between the topology of the physical tree and the phylogenies obtained from the somatic mutations and found no correspondence (Fig. 2c-d, Sup. Note F). These results challenge the expectation in plants that the distribution of mutations corresponds to the branching topology of the tree following the growth of the shoot apical meristems (7). We also found no difference in the number of mutations, the type of mutations (amino acid changes) or the mutation

spectra (mutation context with 5' and 3' amino acids) between the branches exposed to high vs. low light conditions (Fig. 2e-f, Sup. Note G), which suggests a shielding from UVs in the bud layers (10).

As compared to previous reports about somatic mutations in plants (4,10,11), we have detected far more mutations (ten to hundred times more). This discrepancy is likely associated with the methodology (6), since the vast majority of identified somatic mutations had a low allelic fraction, *i.e.* the fraction of genomic reads with the mutation, which indicates the frequency of mutated cells in the analysed sample (Fig. 3a-b, Sup. Note H). The higher total number of mutations detected in *D. guianensis* can be explained by an enrichment in low fraction mutations in the *D. guianensis* tree detected through deeper sequencing (Supplementary Fig. E1), because increasing the number of reads of a genomic region increases the chances of finding a mutation present in only a few cells of a sample. We generalised the result of the predominance of low fraction mutations in two pedunculate oaks (4,10), and an unpublished dataset from one tortuous beech *Fagus sylvatica* using the same methodology (Fig. 3c). We then considered mutations at a high allelic fraction (>0.25), a category of mutations for which methodological differences are expected to have a limited impact. The two tropical trees had 3 and 6 somatic mutations with allelic fraction>0.25, as compared to 56-421 somatic mutations for the reanalysed oaks and beech trees from temperate regions (Fig. 3c). Overall, this suggests that low-frequency mutations account for the vast majority of within-individual somatic diversity in plants (for all species, >90% with f<0.25).

The origin of the somatic mutations' spatial distribution in the physical tree lies in the functioning of the shoot apical meristems. Shoot apical meristems divide either symmetrically into two stem cells or asymmetrically into one stem cell and one differentiated cell (12), resulting in the three-dimensional spatial distribution of stem cells and the somatic mutations they carry during tree growth. In dicots, the layered structure of shoot apical meristems limits cell movement through the prevalence of anticlinal cell divisions, which favours the retention of mutated cell clones, *e.g.* in the form of stable periclinal chimaeras (13). This mechanism could lead to sectoral chimerism through somatic mutations, which may explain both the discrepancy between the physical tree and phylogeny (Fig. 2c-d, 12) and the prevalence of numerous low-frequency somatic mutations (Fig. 3a-b).

Somatic mutations are often viewed as a source of within-tree adaptive variation (14). To test this hypothesis, we investigated whether non-synonymous somatic mutations exhibit differences in allelic fraction as compared to synonymous ones or to non-coding regions. Higher, or lower fractions would be evidence for positive, or negative selection, respectively. On both species, we detected that the average allelic fraction at non-synonymous sites was lower than those at synonymous sites (Fig. 3d). This difference is highly significant in *D. guianensis* but not significant in *S. rubra*, likely because a limited number of mutations was detected (31 synonymous and 9 non-synonymous mutations). This is consistent with the intra-organismal purifying selection of non-synonymous mutations, as also observed in seagrass (14).

Until now, low-frequency somatic mutations have been neglected because they were assumed not to be transmitted, and therefore to have no evolutionary future. We explored the transmission of somatic mutations to the next generation through their redetection in the embryos of developing fruits. We used amplicon resequencing for 160 candidate mutations highly shared

between sampled leaves and branches, including low-frequency mutations. Using stringent quality filters (Sup. Note I), we demonstrated the transmission of 6 out of 97 tested mutations to embryos in *D. guianensis* and 4 out of 25 in *S. rubra* (Fig. 1). The transmitted mutations were found in several branches of the *D. guianensis* tree but in only one branch of the *S. rubra* tree (Fig. 2). Surprisingly, all the mutations for which we found empirical support for their transmission are at low frequency within the plant. Consistently, we observed that the distributions of the allelic fraction of the transmitted mutations (red bars in Fig. 3a-b) were similar to the distributions of the allelic fraction of all mutations in the crown of the trees (yellow bars in Fig. 3a-b, two-sided Student's t-Test t=-0.37 [-0.33, 0.24], df=5.0, p=0.7259 for *D. guianensis* and t = 0.45465 [-0.23, 0.30], df=3.0, p=0.6801 for *S. rubra*), resulting in all transmitted mutations having low allelic fractions. Hence, we found that low-frequency somatic mutations are heritable and thus contribute to increase within-species diversity, which challenges current tacit assumptions that only high-frequency mutations would matter for evolution. Despite their low frequency and scarcity across the genome, low-frequency somatic mutations could substantially contribute to standing genetic variation, which is the engine of evolution (Sup. Note J). We therefore call for a new view on somatic mutations in plants with renewed assumptions: (i) the distribution of somatic mutations does not necessarily correspond to the branching topology of the tree, (ii) most somatic mutations are low-frequency mutations, and (iii) low-frequency mutations can be transmitted to embryos in trees. Our results are consistent with far more complex links between growth, ageing and mutation rates than commonly thought in plants, along the lines of recent empirical evidence in animals (2,15).

Figures

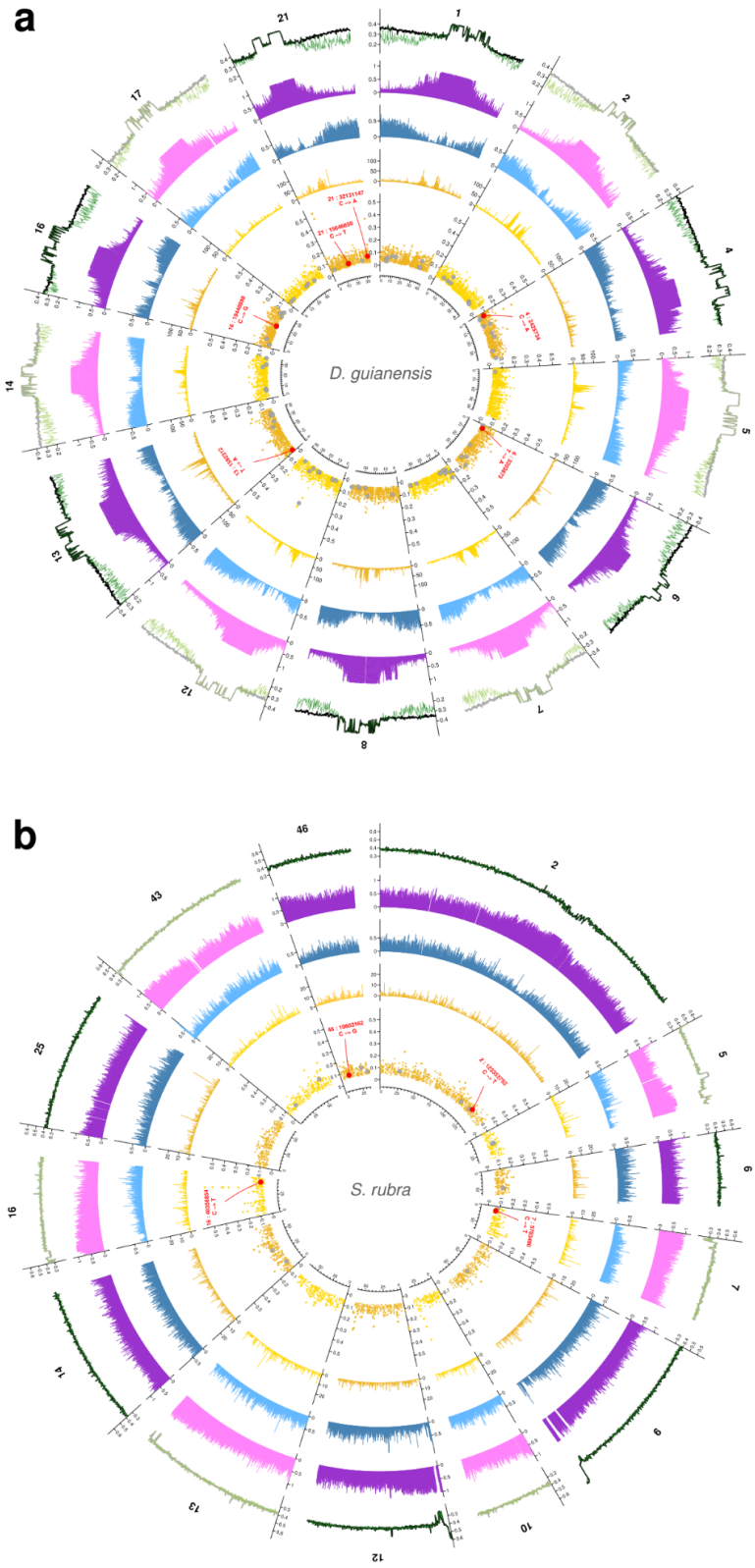
a
D. guianensis
b
S. rubra

Fig. 1 | Crown mutations and transmitted mutations in the genomic landscape of the *Dicorynia guianensis* and the *Sextonia rubra* trees' assembled pseudo-chromosomes. The genomic landscape is similarly portrayed for the two tropical trees: the *Dicorynia guianensis* tree (**a**), and the *Sextonia rubra* tree (**b**). The first (most external) track represents the percentage of Guanine Cytosine (GC) in the whole genome with the black line and in the transposable elements with the green line. The second (least external) track represents the percentage of transposable elements (TE) with purple bars. The third track (middle) represents the percentage of genes with blue bars. The fourth (least internal) track represents the number of somatic mutations detected in the tree crown with yellow bars. The number of somatic mutations correlates with genomic landscapes in *D. guianensis*, the species exhibiting a higher genomic heterogeneity in terms of percentage of genes and TEs (Poisson regression, percentage of TEs b=-0.37(0.04), p<1.10-16, percentage of genes b=-2.31(0.15), p<1.10-16), whereas this is not always significant in *S. rubra* (Poisson regression, percentage of TEs b=-0.62(0.10), p<1.10-9, percentage of genes b=-0.31(0.18), p=0.746). The fifth (innermost) track represents the allelic fraction of the somatic mutations detected in the crown in yellow, the mutations tested for transmission in grey, and the mutations found transmitted to the embryos in red. The inner labels indicate the type of mutations for somatic mutations transmitted to embryos. All measurements are calculated in non-overlapping windows of 100 kb. A ruler is drawn on each pseudo-chromosome, with tick marks every 2 Mb. The genome heterozygosities estimated with K-mer distributions were high for both species, at 0.9% for *D. guianensis* and at 0.7% for *S. rubra*.

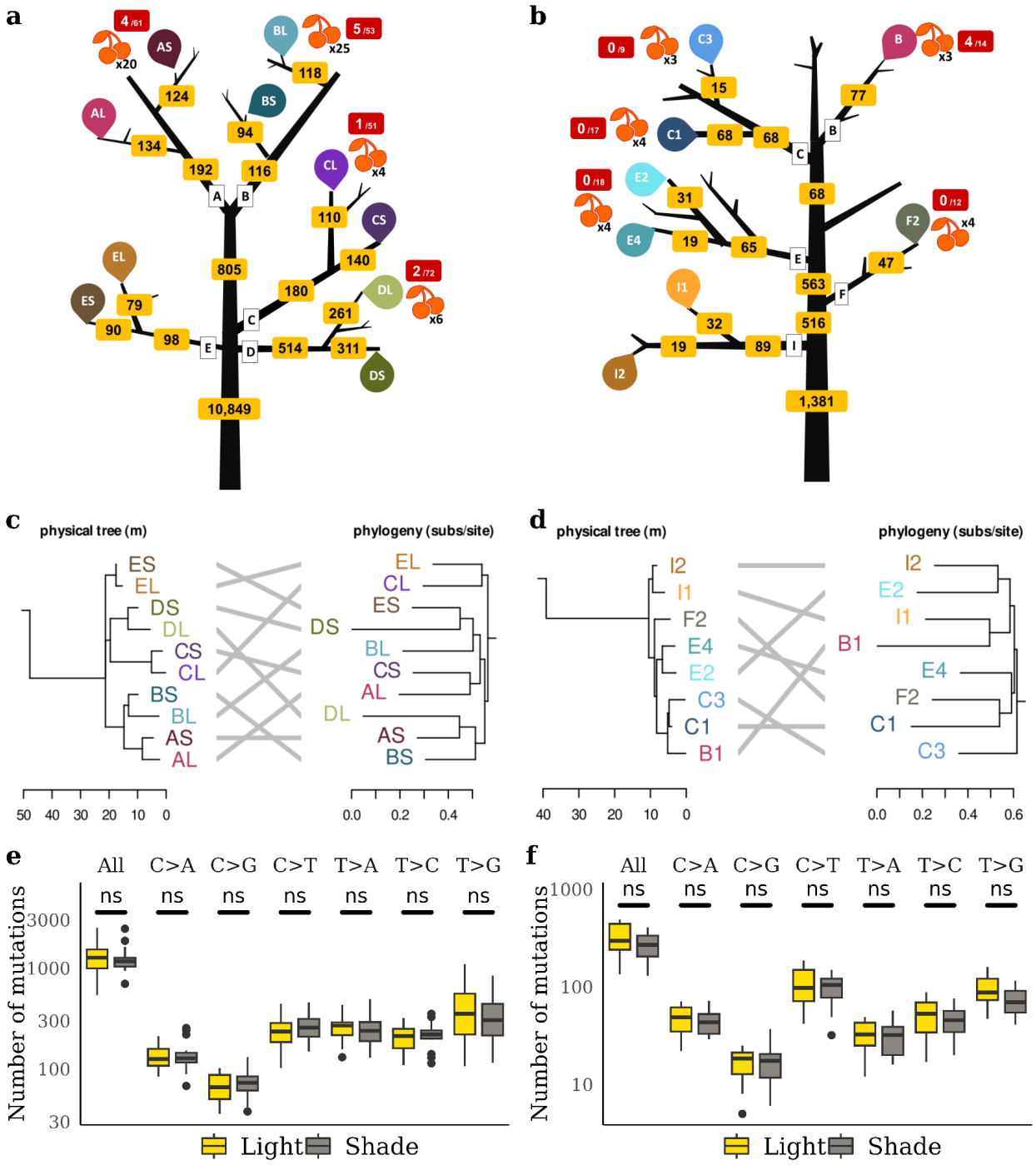

Fig. 2 | Distributions of somatic mutations through branching topology of the tree, phylogenies, and with light. The distributions of somatic mutations through physical trees, phylogenies, and with light are similarly shown for the two tropical trees: the *Dicorynia guianensis* tree (**a,c,e**), and the *Sextonia rubra* tree (**b,d,f**). (**a-b**) The branching topology of the tree is shown in black with the branch names in white boxes. The number of somatic mutations through the crown is indicated in the yellow boxes before the original branching event. The sampling points of three leaves

in the light-exposed branches (“L” in letter codes, light colours) and in the shaded branches (“S”, dark colours) are indicated with unique letter codes and coloured drop symbols. Fruit sampling points are represented by red fruits, with the number of fruits sampled indicated in black. The red boxes with white labels indicate the transmission of mutations to fruit embryos out of the total number of mutations tested. (**c-d**) A side-by-side comparison of the physical tree (left, branch length in metres) and the maximum likelihood phylogeny of mutations (right, branch length in substitutions per site). The letters on the ends of the branches indicate the sampling points shown in (a-b). (**e-f**) Different mutagens may cause specific mutation types, *i.e.,* changing from base X to base Y (X>Y). The effect of light exposure on the accumulation of somatic mutations as a function of mutation type (X>Y) is represented in yellow and grey boxes. The yellow boxes represent the number of mutations accumulated in all leaves of light exposed branches and the grey boxes in all leaves of shaded branches. Boxplots show the median (centre line), upper and lower quartiles (box limits), 1.5x interquartile range (whiskers), and outliers (points). The "ns" labels indicate non-significant differences in Student's t-tests (two-sided). Mutation types include all mutations and all types of transitions and transversions. The y-axis has been scaled logarithmically to facilitate reading of low values.

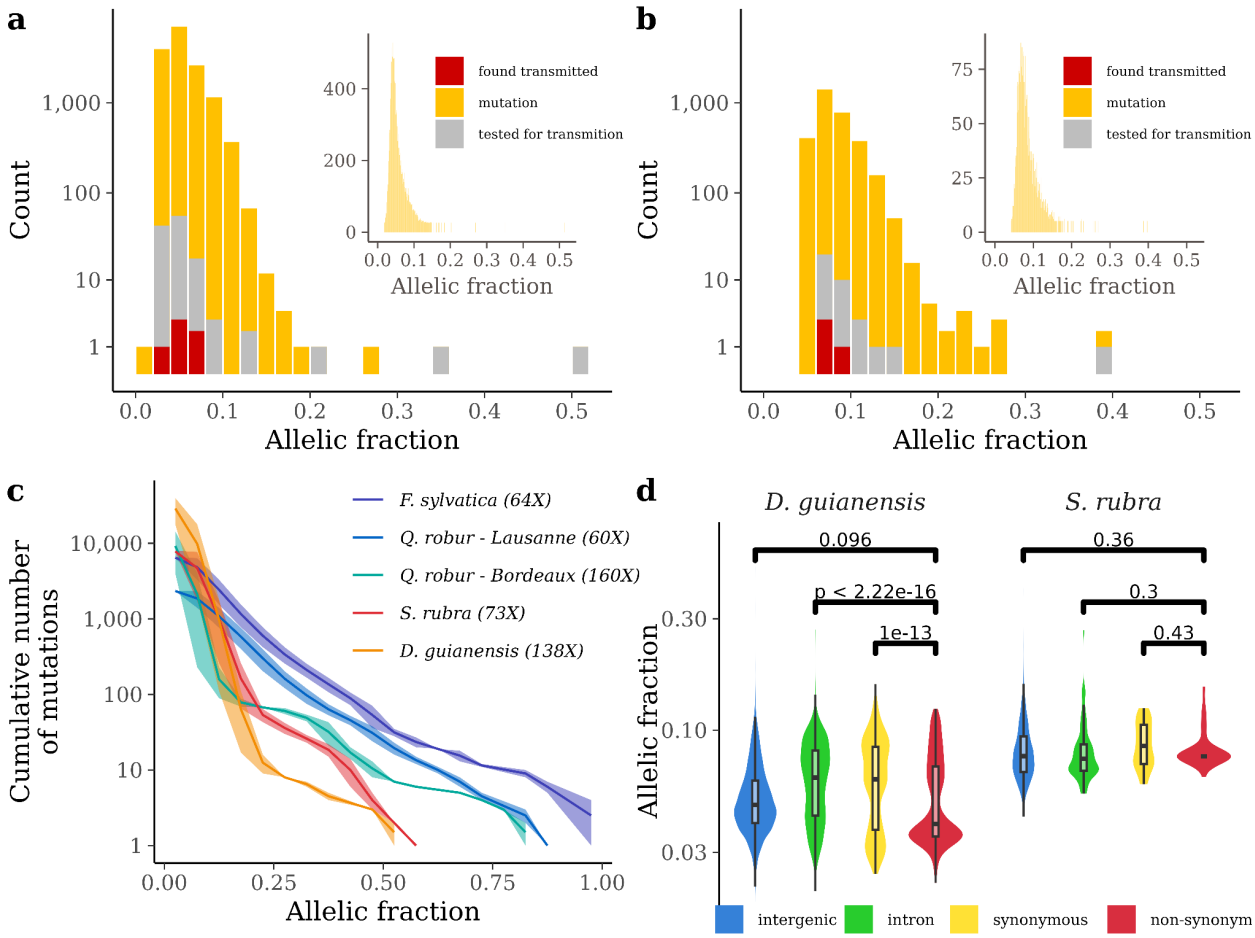

Fig. 3 | Allelic fractions of somatic mutations among trees and among genomic elements. Histogram of allelic fractions of mutations detected in the crown of the two tropical trees: the *Dicorynia guianensis* tree (**a**), and the *Sextonia rubra* tree (**b**). The main histogram shows the allelic fractions of the somatic mutations using a bin of 0.02 and a log-transformed count with the mutations detected in the crown in yellow, the mutations tested for transmission in grey, and the mutations found transmitted to the embryos in red. The inner histogram shows the allelic fractions of the somatic mutations using a bin of 0.001 and a natural count. (**c**) Cumulative number of somatic mutations per branch with decreasing allelic fraction for five trees reanalysed with the same pipeline. The five trees include the two tropical trees studied, the *Dicorynia guianensis* tree in orange and the *Sextonia rubra* tree in red, and three temperate trees, two pedunculate oaks *Quercus robur* L. from Bordeaux in green and Lausanne in blue and a tortuous beech *Fagus sylvatica* L. in purple. All trees were analysed with the same pipeline (see methods) but were sequenced with a different depth indicated in brackets. The line represents the median value while the area represents the minimum and maximum values on the 2 to 10 branches per tree. (**d**) Comparisons of allelic fractions for non-synonymous mutations in red with synonymous mutations in yellow, intronic mutations in green and intergenic mutations in blue for the two tropical trees: the *Dicorynia guianensis* tree (left panel), and the *Sextonia rubra* tree (right panel). Boxplots show the median (centre line), upper and lower quartiles (box limits), 1.5x interquartile range (whiskers), and outliers (points). The p-value above the bars indicates the significance of the Student's T-test (two-sided) for the pairs of groups.

Material and methods

Choice of species and individuals. The study was conducted in the Amazon forest, in the coastal forests of French Guiana. A database of 710 tree species containing available information on the presence of tree rings, maximum diameter at breast height, architectural type, reproductive phenology and ecological and economic importance was constructed. A set of 15 candidate species was selected, and their genome size was estimated by flow cytometric analyses. On this basis, we chose to work on *Dicorynia guianensis* (Amshoff) and *Sextonia rubra* (Mez) van der Werff, which are common in French Guiana, and are ecologically and economically important species. We selected large-stature trees above 40 metres without signs of senescence to maximise the potential for mutations with an increased number of cell divisions. The architecture of the trees was studied with binoculars and by climbing to select trees where in each bough we could sample pairs of branches with contrasting light exposure. We finally selected a *D. guianensis* tree in the Saint George area (4°01'N, 51°59'W), which has an annual rainfall of 3,665 mm and a mean air temperature of 27°C, and a *S. rubra* tree near the Paracou research station (5°18'N, 52°53'W), which has an average annual rainfall of 3,041 mm and a mean air temperature of 25.7°C (Sup. Note A).

Genome assemblies and annotations. High molecular weight (HMW) DNA was extracted from 0.7 g of three leaves of both individuals using CTAB and isopropanol precipitation before RNAase treatment and bead purification (Doyle and Doyle 1987). High-fidelity (HiFi) genomic reads were produced with two sequencing runs on the PacBio Sequel II system on 2 (*D. guianensis*) to 4 (*S. rubra*) SMRTCells for each run. We obtained 1,898,004 corrected reads for *D. guianensis* (N50=21,233; DP=58.7X), which we assembled into 562 contigs (N50=37.76Mb; L50=8 contigs;

GC=37.25%) using the HiFiasm assembler (v0.15.5). Similarly, we obtained 6,624,997 corrected reads for S. rubra (N50=17,577; DP=114X), which we assembled into 747 contigs (N50=16.513Mb; L50=17 contigs; GC=38.50%). HMW DNA was also used to produce optical maps for the hybrid scaffold with optical reads produced by two passages of Bionano saphyr. For *D. guianensis*, we obtained 54 hybrid scaffolds (N50=38,450Mb; N=0.76%; 571 gaps), while 515 contigs remained unanchored with a total length of 28,784Mb representing 4.97% of the genome. For *S. rubra*, we obtained 35 hybrid scaffolds (N50=60.458Mb; N=1%; 1.923 gaps), while 609 contigs remained unanchored with a total length of 53.067Mb representing 5.08% of the genome. We constructed an automated genome annotation workflow that performs: (i) de novo and known transposable element (TE) detection, (ii) de novo and known gene models detection, and (ii) functional gene annotation. De novo TE detection uses RepeatModeler2 (v2.0.3) followed by classification using RepeatClassifier (v2.0.3) and TEclass (v2.1.3). The de novo TEs obtained are merged with the known TE accessions for Viridiplantae from RepBase (v27.07). This consolidated database is used for TE detection in each genome prior to soft masking using RepeatMasker (v2.0.3). Detection of de novo and known gene models is based on BRAKER2 and its dependencies. Finally, functional annotation of candidate genes is based on the Trinotate (v3.2.1) pipeline using TransDecoder (v5.5.0), TMHMM, HMMER, BLAST (v2.13.0), RNAmmer (v1.2), and SignalP (v4.1) with UniProt and Pfam databases (Sup. Note B).

Sampling. On 13 October 2020, we sampled the tree *S. rubra*: three cambium tissues at the base of the trunk, about 1.3 m above the ground and equidistant around the perimeter of the trunk; three leaves from the same twig per branch out of eight branches were sampled, the branches were selected in three pairs, each from a different bough, plus two independent branches from two other boughs; and fruits from 5 different branches where leaves had been collected. On 22 April 2021, we sampled the *D. guianensis* tree: three cambium tissues at the base of the trunk, about 1.3 m above the ground and equidistant from the perimeter of the trunk; three leaves from a single twig per branch of ten branches were sampled, the branches were selected in five pairs of branches each from a different bough; and fruits from 5 different branches where leaves were collected. On 13 October 2020 and 15, 16 and 22 November 2021, we described the structure of both trees: all branch lengths, as well as basal and terminal diameters, were measured for branches with a basal diameter greater than 10 cm, in addition to the trunk. On 21, 22 and 23 March 2022, 30 wood cores were taken with a drill through the crown and into the trunk of *D. guianensis*. In both species, leaf, cambium, and fruit samples were frozen in liquid nitrogen and stored at -80ºC until DNA and RNA extraction (Sup. Note C).

Characterisation of light conditions. A linear PAR ceptometer (AccuPar, Decagon Devices, Pullman, WA, USA) was used at each sampling position on both trees during sampling to measure direct incident light in the 400-700 nm wavelength range around noon in comparison to open incident light measured on the nearest road. A ground and UAV lidar campaign (TLS, Faro Focus3D 120; DLS, Yellowscan Vx20-100) was conducted on 3 May 2021 to map the transmittance of the *D. guianensis* tree canopy. TLS scans were performed horizontally from 0 to 360° and vertically from -60 to 90°, resulting in 174.8 million points per scan for 10 scans in a forest gap near the tree and 4 scans from the nearby road. DLS scans were taken at 35 m above the focal tree in 2 perpendicular flights with flight lines spaced 10 m apart in a circular area 150 m in diameter above the focal tree,

resulting in 46.6 million points. Prior to the lidar acquisition, reflective strips were placed on the sample points by tree climbers to detect the sample points in the lidar cloud. AMAPvox software was used to calculate an annual illuminance index from the aerial laser scanning. The plant area density (PAD, m2/m3) was calculated for the focal tree in context (with a diameter of 30 m around the tree) using 1 m3 voxels. An estimate of the annual proportion of solar radiation above the canopy received at the sample point was then simulated considering a brightness index of 0.5 and a latitude of 5 degrees. The uncertainty in transmittance due to uncertainties in the location of the sampling point was further assessed by randomly sampling 10 positions around the sampling points to 0.5 metres and revealed small variations in transmittance. The estimates were in agreement with the light/shade classification of branches identified by the tree climbers (Sup. Note D).

Leaf and cambium mutation detection. Genomic DNA was extracted from 30 mg of frozen leaf or cambium tissue per sample point for both trees using a CTAB protocol with chloroform-isoamyl alcohol extraction (24:1), isopropanol precipitation and resuspension of the pellet in 1x Low TE (10 mM Tris-HCl + 0.1 mM EDTA). DNA was quantified using a Qubit HS assay (Thermo Fisher Scientific, Waltham, MA, USA) and purified with AMPure XP beads (Beckman Coulter Genomics, Danvers, MA, USA) where necessary to allow library preparation. An Illumina sequencing library was produced for each leaf using an optimised NEBNext Ultra II DNA library protocol (New England Biolabs, Ipswich, MA, USA). Libraries were pooled into multiplexes after each library was independently labelled prior to whole genome sequencing (WGS) on an S4 flow cell and NovaSeq 6000 instrument with v1.5 chemistry (2 x 150 PE mode). We obtained 33 cambium and leaf libraries for *D. guianensis* with a sequencing depth of about 160X and 27 libraries with a depth of about 80X for *S. Rubra*. We took advantage of a workflow to detect somatic mutations from sequencing reads mapped to a genomic reference (6). Paired sequencing reads from each library are quality controlled using FastQC (v0.11.9) before being trimmed using Trimmomatic (v0.39), which retains only paired-end reads without adapters and with a phred score greater than 15 in a 4-base sliding window. The reads are aligned against the reference genome using BWA mem with the option to mark shorter splits (v0.7.17). The alignments are then compressed using Samtools view in CRAM format, sorted by coordinates using Samtools sort, and indexed using Samtools index (v1.10). Duplicate reads in the alignments are marked using GATK MarkDuplicates (v4.2.6.1). Sequencing depth is estimated along the genome using Mosdepth (v0.2.4) globally and over a sliding window of 1 kb. We used Jellyfish (v1.1.12) and GenomeScope to estimate heterozygosity up to 21-mer. We used GATK (HaplotypeCaller, GatherGVCFs, GenomicsDBImport, GenotypeGVCFs) to call heterozygous sites from the previously obtained alignments. We filtered single-nucleotide polymorphisms (SNPs) using bcftools (v1.10.2), GATK VariantFiltration (v4.2.6.1), and plink (v1.90), retaining only biallelic SNPs with quality less than 30, quality per depth less than 2, Fisher strand ratio greater than 60, and strand odds ratio greater than three. To eliminate all truly heterozygous sites, we further filtered out SNPs present in all sampled genotypes and tissues (no missing data) and shared by at least all but one tissue. Finally, the workflow uses Strelka2 (v2.9.10) to detect mutations by comparing two samples, a mutated sample and a normal (directional) sample. To detect cambium mutations present at the base of the tree, we compared all potential pairs (6 in total) among the three cambium libraries. To detect leaf mutations, we compared each leaf library to the first cambium library as a reference sample. We filtered out candidate leaf mutations from previously identified heterozygous sites and all candidate mutations from all cambium comparisons using BEDTools subtract (v2.29.2). We also

filtered mutations using the following criteria: (i) no copies of the mutated allele in the reference sample, in this case the cambium sample; (ii) a read depth for both samples between the 5th quantile and the 95th quantile of the corresponding library coverage; and (iii) the presence of the mutation in at least two biological replicates (at least 2 leaves of the crown) We used the same pipeline and compared mutations detected in two pedunculate oaks *Quercus robur* (4,10), and in an unpublished dataset from a twisted beech *Fagus sylvatica* (J.M. Aury and C. Plomion pers. com.) (Sup. Note E).

Somatic mutation distributions through physical trees, phylogenies, and with light. We explored mutation distribution along tree architecture by assuming the origin of the mutation in the tree architecture was at the latest the most recent common branching event among all branches harbouring the mutation (11). We further built mutation phylogenies using iqtree rooting the tree with the non-mutated library from the cambium mean genotype without mutations. We compared phylogenies to the physical architecture of both trees with the dendextend R package (Supplementary Note F). We explored the effects of light on the occurrence of mutations in the trees using Student's T-tests and Kolmogorov-Smirnov tests. We compared the number of mutations detected in branches exposed to high vs. low light conditions using the leaves as an observation. We further compared mutation types (base change) and mutation spectra (mutation context with 5' and 3' bases) between high and low light conditions among branches of each tree (Sup. Note G).

Low-frequency mutations annotation. We explored the allelic fractions of somatic mutations in relation to tree sequencing depth, a known determinant of the sensitivity of somatic mutation detection (8), for the *D. guianensis* tree, the *S. rubra* tree, two pedunculate oaks *Quercus robur* (4,10), and unpublished data from one tortuous beech *Fagus sylvatica* (C. Plomion pers. com.). We further compared mutation annotations in terms of their presence in transposable elements (TE) and genes among trees. We assessed mutation functional impact using SNPeff and related non-synonymous mutations to their functional annotations, gene ontology, and allelic fraction. We finally explored the allelic fraction of mutations depending on genomic contexts using Student T tests (Sup. Note H).

Detection of fruit mutations. We explored mutation transmission to fruit using amplicon resequencing. We kept as candidate mutations for redetection only mutations present in at least three leaves from the branches that had fruits during sampling for resequencing, which resulted in 160 candidate mutations (124 for *D. guianensis* and 36 for *S. rubra*). Frozen fruits were dissected in 4 tissues: (i) embryo sac, (ii) nucellus, (iii) pericarp, and (iv) fruit base. Genomic DNA was extracted from 10-50 mg of frozen fruit tissue for both trees and additional leaf tissue for positive control with a CTAB protocol with chloroform - isoamyl alcohol (24:1) extraction, isopropanol precipitation and pellet resuspension in 1x Low TE (10 mM Tris-HCl + 0.1 mM EDTA; Doyle and Doyle 1987). DNA was quantified using a Qubit HS assay. Primer3plus was used to design primer pairs targeting candidate mutations (amplicon size between 100 and 200 pb). Only one *D. guianensis* candidate mutation failed to yield a primer pair. Illumina universal tags were added to the 5′ end of the forward and reverse primer sequences respectively. Oligonucleotides were ordered in a plate format from Integrated DNA Technologies (Coralville, IA, USA) with standard desalt purification at 25 nmoles synthesis scale. Each primer pair was tested using simplex PCR amplification of one DNA sample per species in a volume of 10 µL containing 2 µL of 5X Hot Firepol Blend master mix (Solis Biodyne,

Tartu, Estonia), 1 µL of 2µM primer pairs, 1 µL of DNA (10 ng/µL), and 6 µL of PCR-grade water. We run the PCR on a Veriti 96-Well thermal cycler (Applied Biosystems, Waltham, MA, USA) which consisted in an initial denaturation at 95°C for 15 min, followed by 35 cycles of denaturation at 95°C for 20 s, annealing at 59°C for 60 s, extension at 72°C for 30s, and a final extension step at 72°C for 10 min. We checked the amplification on a 3% agarose gel. A total of 6 *D. guianensis* primer pairs that failed to amplify were discarded at this stage. The remaining 101 *D. guianensis* and 33 *S; rubra* primer pairs, targeting respectively 117 and 36 mutations, were grouped accounting for potential primer dimer formation using PrimerPooler for subsequent multiplex PCR amplification. Four multiplexed PCR were done for each species in a volume of 10µL using 2 µL of 5X Hot Firepol Multiplex master mix (Solis Biodyne), 1 µL of multiplex primer mix (0.5 µM of each primer), 2 µL of DNA (10 ng/µL), and 5 µL of PCR-grade water. The amplification was carried on a Veriti 96-Well thermal cycler (Applied Biosystems) using an initial denaturation at 95°C for 12 min followed by 35 cycles of denaturation at 95°C for 30 s, annealing at 59°C for 180 s, extension at 72°C for 30 s, and a final extension step at 72°C for 10 min. The amplicons from the four multiplexed PCR of each sample were pooled. Illumina (San Diego, CA, USA) adapters and sample-specific Nextera XT index pairs were added to the amplicons by a PCR targeting the Illumina universal tags attached to the locus-specific primers. This indexing PCR was done in a volume of 20 µL using 5X Hot Firepol Multiplex master mix , 5 µL of amplicon, and 0.5 µM of each of the forward and reverse adapters, using an initial denaturation at 95°C for 12 min followed by 15 cycles of denaturation at 95°C for 30 s, annealing at 59°C for 90 s, extension at 72°C for 30 s, and a final extension step at 72°C for 10 min. We then pooled the libraries and purified them with 0.9X AMPure XP beads (Beckman Coulter, Brea, CA, USA). We checked the library quality on a Tapestation 4200 (Agilent Technologies, Santa Clara, CA, USA) and quantified it using QIAseq Library Quant Assay kit (Qiagen, Hilden, Germany) ona LightCycler 480 quantitative PCR (Roche, Basel, Switzerland). The sequencing was done on an Illumina MiSeq sequencer using a V2 flow cell with a 2x150 bp paired-end sequencing kit. We analysed the amplicon resequencing using FDSTools embedded into a pipeline used to format results, to compare blind-repeated genotyping to estimate genotyping error rate and to extract locus and allele information. We further aligned consensus contigs of each haplotype on corresponding genomes with BWA mem v0.7.17 and classified the status of mutations on each haplotype by manually examining the alignment on IGV. We explored mutation transmission with strict detection and filtering of mutations in fruit tissues. We evaluated the transmission of somatic mutations with the highest stringency by removing: (1) suspect mutations based on genomic area inspection after consensus haplotypes alignments; (2) mutations inconsistent with branch origin; and (3), mutations inconsistent among fruit tissues. Mutations were classified as (1) verified, i.e. identified in a realigned haplotype, (2) not redetected, i.e. corresponding haplotypes only had the reference allele, (3) unaligned, i.e. the amplicon did not cover the targeted genomic area, or (4) other cases, including mainly candidate mutations close to a poly-A repeat and one candidate mutation suspected to be a paralog. We then focused on the mutations transmitted to fruits embryos and further filtered by checking: (1) the consistency between the origin of the mutation in the tree crown for the original leaves where it was detected with the origin of the fruit in the tree crown; and, (2) the consistency between the fruit tissues, mainly whether the genotype of the cotyledon and embryo sac matched. We finally explored the relation between the rate of transmission of mutations to embryos and the median of the allelic fraction of mutation in leaves from their respective branches and in the whole crown with a Pearson's correlation test (Sup. Note I).

Data, script and code availability

Genomic and transcriptomic reads from leaf, cambium, and fruits and corresponding genomes are available in GenBank (16). genomeAnnotation and detectMutations pipelines as well as downstream analyses are available on GitHub (17-20). Results and intermediary files are available on Zenodo (21).

Acknowledgments

We are grateful to Valentine Alt, Emeline Houël, Laetitia Brechet, Saint-Omer Cazal, and Hadrien Lalagüe for their help with tree climbing and sampling. We thank Olivier Brunaux and Caroline Bedeau for their help in accessing the site and the forest office data. We are grateful to Nicolas Barbier, Ilona Clocher, and Jean-Louis Smock for their help with lidar acquisition. PacBio HiFi reads were produced at Gentyane platform and Lausane platform for *S. rubra* and *D. guianensis* , respectively. Bionano Saphir reads and genome de-novo assembly were produced at CNRGV. Whole genome sequencing was performed at Genoscope with the help of Eric Mahieu, Corinne Cruaud, and Pedro H. Oliveira. Sequence-based genotyping was performed at PGTB (doi:10.15454/1.5572396583599417E12) with the help of Zoé Delporte. We are grateful to the genotoul bioinformatics platform Toulouse Occitanie (doi:10.15454/1.5572369328961167E12) for providing help and/or computing and/or storage resources The climate data were provided by Météo-France to the Unité Mixte de Recherche EcoFoG for research purposes within the framework of a MétéoFrance-INRAE AgroClim agreement. This study was funded by an ANR Investissement d'Avenir grant: CEBA (ANR-10-LABEX-0025).

Competing interests

The authors declare no competing interests.

Authors' contributions

NT, MH, TL, CP, JC, and PH conceived the ideas; VT, JC, NT, PH, and SS realised the fieldwork; GV and OM characterised individuals light conditions; MB, EC, CC, EG, OL, JL, WM, VT, and MH produced genetic data; SS, TL, NT, and MH both analysed the data and led the writing of the manuscript. All authors contributed critically to the drafts and gave final approval for publication.

References

1. Weismann, A. (1893). *The Germ-plasm: A Theory of Heredity*.
2. Bergeron, L. A., Besenbacher, S., Zheng, J., Li, P., Bertelsen, M. F., Quintard, B., Hoffman, J. I., Li, Z., st. Leger, J., Shao, C., Stiller, J., Gilbert, M. T. P., Schierup, M. H., & Zhang, G. (2023). Evolution of the germline mutation rate across vertebrates. *Nature*. https://doi.org/10.1038/s41586-023-05752-y
3. Lanfear, R. (2018). Do plants have a segregated germline? *PLoS Biology*, *16*(5), 1–13. https://doi.org/10.1371/journal.pbio.2005439
4. Plomion, C., Aury, J. M., Amselem, J., Leroy, T., Murat, F., Duplessis, S., Faye, S., Francillonne, N., Labadie, K., le Provost, G., Lesur, I., Bartholomé, J., Faivre-Rampant, P., Kohler, A., Leplé, J. C., Chantret, N., Chen, J., Diévart, A., Alaeitabar, T., … Salse, J. (2018). Oak genome reveals facets of long lifespan. *Nature Plants*, *4*(7), 440–452. https://doi.org/10.1038/s41477-018-0172-3
5. Wang, L., Ji, Y., Hu, Y., Hu, H., Jia, X., Jiang, M., Zhang, X., Zhao, L., Zhang, Y., Jia, Y., Qin, C., Yu, L., Huang, J., Yang, S., Hurst, L. D., & Tian, D. (2019). The architecture of intra-organism mutation rate variation in plants. *PLoS Biology*, *17*(4), 1–29. https://doi.org/10.1371/journal.pbio.3000191
6. Schmitt, S., Leroy, T., Heuertz, M., & Tysklind, N. (2022). Somatic mutation detection: a critical evaluation through simulations and reanalyses in oaks. *Peer Community Journal*, *2*, e68. https://doi.org/10.24072/pcjournal.187
7. Orr, A. J., Padovan, A., Kainer, D., Külheim, C., Bromham, L., Bustos-Segura, C., Foley, W., Haff, T., Hsieh, J. F., Morales-Suarez, A., Cartwright, R. A., & Lanfear, R. (2020). A phylogenomic approach reveals a low somatic mutation rate in a long-lived plant. *Proceedings of the Royal Society B*. https://doi.org/10.1098/rspb.2019.2364
8. Holá, M., Vágnerová, R., Angelis, K. J. (2015). Mutagenesis during plant responses to UVB radiation. *Plant Physiology and Biochemistry*, 93, 29–33. https://doi.org/10.1016/j.plaphy.2014.12.013
9. Kim, S., Scheffler, K., Halpern, A. L., Bekritsky, M. A., Noh, E., Källberg, M., Chen, X., Kim, Y., Beyter, D., Krusche, P., & Saunders, C. T. (2018). Strelka2: fast and accurate calling of germline and somatic variants. *Nature Methods*, *15*(8), 591–594. https://doi.org/10.1038/s41592-018-0051-x
10. Schmid-Siegert, E., Sarkar, N., Iseli, C., Calderon, S., Gouhier-Darimont, C., Chrast, J., Cattaneo, P., Schütz, F., Farinelli, L., Pagni, M., Schneider, M., Voumard, J., Jaboyedoff, M., Fankhauser, C., Hardtke, C. S., Keller, L., Pannell, J. R., Reymond, A., Robinson-Rechavi, M., … Reymond, P. (2017). Low number of fixed somatic mutations in a long-lived oak tree. *Nature Plants*, *3*(12), 926–929. https://doi.org/10.1038/s41477-017-0066-9
11. Duan, Y., Yan, J., Zhu, Y., Zhang, C., Tao, X., Ji, H., Zhang, M., Wang, X., & Wang, L. (2022). Limited accumulation of high-frequency somatic mutations in a 1700-year-old Osmanthus fragrans tree . *Tree Physiology*, 1–10. https://doi.org/10.1093/treephys/tpac058
12. Bowman, J. L., & Eshed, Y. (2000). Formation and maintenance of the shoot apical meristem. *Trends in Plant Science*, *5*(3), 110–115. https://doi.org/10.1016/S1360-1385(00)01569-7

13. Burian, A. (2021). Does Shoot Apical Meristem Function as the Germline in Safeguarding Against Excess of Mutations? In *Frontiers in Plant Science* (Vol. 12, Issue August, pp. 1–9). https://doi.org/10.3389/fpls.2021.707740
14. Yu, L., Boström, C., Franzenburg, S., Bayer, T., Dagan, T., & Reusch, T. B. H. (2020). Somatic genetic drift and multilevel selection in a clonal seagrass. *Nature Ecology & Evolution*, 4(7), 952–962. https://doi.org/10.1038/s41559-020-1196-4
15. Cagan, A., Baez-Ortega, A., Brzozowska, N., Abascal, F., Coorens, T. H., Sanders, M. A., …, Martincorena, I. (2022). Somatic mutation rates scale with lifespan across mammals. *Nature*, 604, 517-524. https://doi.org/10.1038/s41586-022-04618-z
16. Schmitt, S., Heuret, P., Troispoux, V., Beraud, M., Cazal, J., Chancerel, E., Cravero, C., Guichoux, E., Lepais, O., Loureiro, J., Marande, W., Martin, O., Vincent, G., Chave, J., Plomion, C., Leroy, T., Heuertz, M., Tysklind, N. (2023). Mutation in the tropical tree canopy: genomic and transcriptomic reads from leaf, cambium, and fruits and corresponding genomes. *GenBank* BioProject PRJNA823677. https://dataview.ncbi.nlm.nih.gov/object/PRJNA823677
17. Schmitt, S. (2023). sylvainschmitt/genomeAnnotation: v0.1.0. *Zenodo*. https://doi.org/10.5281/zenodo.7993843
18. Schmitt, S. (2023). sylvainschmitt/detectMutations: Angela 0.1.0. *Zenodo*. https://doi.org/10.5281/zenodo.7994237
19. Schmitt, S. (2023). sylvainschmitt/detectMutations: Sixto 0.1.0. *Zenodo*. https://doi.org/10.5281/zenodo.7994249
20. Schmitt, S. (2023). sylvainschmitt/treemutation: 1.0.0. *Zenodo*. https://doi.org/10.5281/zenodo.7994454
21. Schmitt, S., Leroy, T., Heuertz, M., Tysklind, N. (2023). Low-frequency somatic mutations are heritable in plants: Data set. *Zenodo*. https://doi.org/10.5281/zenodo.7994906

Supplementary Material for:

Low-frequency somatic mutations are heritable in plants

Sylvain Schmitt[1,2,*], Patrick Heuret[2], Valérie Troispoux[3], Mélanie Beraud[4], Jocelyn Cazal[3], Émilie Chancerel[5], Charlotte Cravero[6], Erwan Guichoux[5], Olivier Lepais[5], João Loureiro[7], William Marande[6], Olivier Martin[8], Gregoire Vincent[2], Jérôme Chave[9], Christophe Plomion[5], Thibault Leroy[10,11,+], Myriam Heuertz[5,+], Niklas Tysklind[3,+]

[1]CNRS, UMR EcoFoG (Agroparistech, Cirad, INRAE, Université des Antilles, Université de la Guyane), Campus Agronomique, 97310 Kourou, French Guiana;[2]AMAP, Univ. Montpellier, CIRAD, CNRS, INRAE, IRD, Montpellier, France;[3]INRAE, UMR EcoFoG (Agroparistech, CNRS, Cirad, Université des Antilles, Université de la Guyane);[4]Genoscope affiliation;[5]Univ. Bordeaux, INRAE, BIOGECO, 69 route d'Arcachon, CS 80227, 33612 Cestas Cedex; [6]INRAE, (CNRGV French Plant Genomic Resource Center, F-31320, Castanet Tolosan, France);[7]Centre for Functional Ecology, Department of Life Sciences, University of Coimbra, Calçada Martim de Freitas, 3000-456, Coimbra, Portugal;[8]URFM, INRAE, 84000 Avignon, France; [9]Laboratoire Evolution et Diversité Biologique, UMR5174, CNRS, Université Paul Sabatier, IRD, Toulouse Cedex 9, France; [10]Department of Botany and Biodiversity Research, University of Vienna, Rennweg 14, A-1030 Vienna, Austria; [11]GenPhySE, INRAE, INP, ENVT, Université de Toulouse, 24 chemin de Borde-Rouge - Auzeville Tolosane, 31326 Castanet Tolosan;[*] E-mail: sylvain.m.schmitt@gmail.com;[+] T.L., M.H., and N.T. contributed equally to this work.

Table of content

Table of content
A - Choice of species and individuals
B - Genome assemblies and annotations
C - Sampling
D - Characterisation of light conditions
E - Leaf and cambium mutation detection
F - Mutations along the tree architecture
G - Light and somatic mutations
H - Low-frequency mutations
I - Fruit mutations redetections
J - Somatic mutations and population diversity
References

A - Choice of species and individuals

Candidate species selection

To study the process of mutations, we wanted to focus on a species that fulfilled a maximum of these criteria:

- Ecological relevance: we aimed to work on common species, so the results of our study would be ecologically relevant.
- Economic relevance: we aimed to work on species where the availability of high quality genomes would contribute to further studies on genomics, evolutionary ecology, and sustainable management of these species.
- Species tree architecture: we aimed to have emergent canopy trees with typical architectures that allowed us to establish a sampling design where pairs of branches with contrasting sun exposure could be sampled on the same bough, and this sampling strategy repeated on different boughs across the whole tree canopy.
- Predictable phenology: we aimed to study species where we could predictably expect fruits for the individual tree, so that we could assess the transmission of mutations from somatic tissues to the embryo tissues.
- Genome size: we aimed to work on species with smaller genomes, which would reduce the amount of sequencing needed to identify low-frequency mutations.

The study was conducted in the Amazon forest, in the coastal forests of French Guiana. A database of 710 species of trees from French Guiana containing information on the functional group, maximum diameter at breast height, architectural model, presence of wood rings, reproductive phenology, and ecological and economical importance was constructed. A set of 15 candidate species was thus selected based on these criteria.

Genome size estimation

To obtain information on genome size of the candidate species we collected leaf tissue from 15 individuals from the 15 selected species at Paracou Research station, and conserved the tissues in RNAlater (Qiagen) or in silica gel until flow cytometric analyses. Nuclear suspensions were obtained following Galbraith et al. (1983) by chopping RNA-later conserved tissue of the studied species and fresh leaf tissue of *Pisum sativum* 'Ctirad' (internal reference standard, 2C = 9.09 pg; Doležel et al. 1998) in 1 ml of WPB buffer (Loureiro et al. 2007). Then, the nuclear suspension was filtered using a 50 µm nylon mesh and 50 µg/ml of propidium iodide (PI, Fluka, Buchs, Switzerland) and 50 µg/ml of RNAse (Fluka, Buchs, Switzerland) were added to stain the nuclear DNA and remove dsRNA, respectively. Samples were analysed in a Sysmex CyFlow Space flow cytometer equipped with a 532 nm green solid-state laser and operating at 30 mW, and results were acquired using FloMax software v2.4d.

Regardless of whether preserved in RNAlater or in silica gel, we were able to obtain reliable haploid genome size estimates ranging from 419 Mbp (in *Laetia procera*) to 1836 Mbp (in *Symphonia globulifera*) (Table A1). According to the genome size categories of Leitch et al.

(1998), most of the candidate species present a very small genome size (1C ≤ 1,372 Mbp). Only *Moronobea coccinea* with 1C = 1508 Mbp and *Symphonia globulifera* with 1C = 1,836 Mbp, presented a small genome size. The genome size estimation of *Eschweilera coriacea* obtained here is slightly larger than the one given in Heuertz et al. (2020), but it is in the same range of values as other estimations obtained in the genus (Heuertz et al., 2020).

Table A1: Characteristics of the 15 candidate species: ***Family***, ***genus***, *and* ***species*** *names are tabulated;* ***An. rings****: The occurrence of annual rings either in the species, or in other species in the genus;* ***Rep. phen****.: if the reproductive phenology is known, we indicate if its is annual (A), biennial (B), or supra-annual (S-A);* ***Arch. Model:*** *the typical architecture model of the species;* ***GS (Mbp):*** *the size of the 1C haploid genome in mega base pairs (Mbp);* ***Ind****.: sampling location and individual identifier at the Paracou Station (P: Parcelle; C: carré; Ind: individual).*

Family	Genus	Species	ring	Rep. phen.	Arch. Model	GS (Mbp)	Ind.
Bignoniaceae	*Handroanthus*	*serratifolius (Vahl) S.O. Grose*	S		Koriba (Hot,1978)	572	P_6, C_2, Ind_431
Caryocaraceae	*Caryocar*	*glabrum (Aubl.)*	S	A	Scaronne (Vester & Cleef, 1998)	899	P_6, C_2, Ind_716
Clusiaceae	*Moronobea*	*coccinea (Aubl.)*	S	A; B	Massart (Keller, 1994)	1508	P_6, C_2 Ind_776
Clusiaceae	*Platonia*	*insignis (Mart.)*	S	B	Massart (Hot, 1978)	1748	P_14, C_3, Ind_112
Clusiaceae	*Symphonia*	*globulifera (L.)*	S	A	Massart (Hot, 1978; Barthélémy, 1988)	1836	P_6, C_4, Ind_2941
Dichapetalaceae	*Tapura*	*capitulifera (Baill.)*	G		Cook (Hot, 1978)	948	P_6, C_2, Ind_2919
Fabaceae	*Dicorynia*	*guianensis (Amshoff)*	S	S-A	(Drénou, 1988)	691	P_6, C_2, Ind_898
Fabaceae	*Vouacapoua*	*americana (Aubl.)*	S	S-A	Troll (Hot, 1978)	1028	P_6, C_2, Ind_387
Goupiaceae	*Goupia*	*glabra (Aubl.)*	S		Roux (Hot, 1978)	482	P_6, C_2, Ind_774
Lauraceae	*Sextonia*	*rubra (Mez) van der Werff*	no		Aubréville (Laurans & Vincent 2016)	1354	P_6, C_3, Ind_2353
Lecythidaceae	*Eschweilera*	*coriacea (DC.) S.A. Mori*	no		Troll (Obs. Caraglio & Nicolini)	1040	P_6, C_2, Ind_876
Myristicaceae	*Virola*	*michelii (Heckel)*	G		Massart (Hot, 1978)	1051	P_6, C_2, Ind_2812
Salicaceae	*Laetia*	*procera (Poepp.) Eichler*	no		Roux (Drénou, 1994)	419	P_6, C_2, Ind_790
Sapotaceae	*Pradosia*	*Cochlearia (Lecomte) T.D.Penn.*	no		Aubréville (Laurans & Vincent 2016)	983	P_6, C_2, Ind_766
Vochysiaceae	*Qualea*	*rosea (Aubl.)*	no		Massart (Obs. Caraglio & Nicolini)	1179	P_6, C_2, Ind_607

Based on all of the above information we chose to work on *Dicorynia guianensis* (Amshoff) and *Sextonia rubra* (Mez) van der Werff, which are common in French Guiana, and they are

ecologically and economically important species, being respectively the first and second most harvested species in French Guiana. They are shade-tolerant, canopy to emergent trees. *D. guianensis* forms growth-rings (Detienne 1995), while *S. rubra* produces seasonal variation in wood chemistry (Ponton *et al.*, 2016). Both species have very small genomes.

Individual selection

We surveyed *D. guianensis* trees at the Paracou research station and the Office National des Forêts plots between Régina and Saint George (Secteur Saint George). We aimed to find trees as large as possible (DBH > 100cm) but without evidence of senescence. This was to maximise the potential of mutations, assuming that the number of mutations is correlated with the number of cellular divisions. We avoided senescent trees that may have lost many of their main branches, as well as trees with evidence of damage from nearby treefalls, or trees whose crowns were intermingled with other trees. We examined the architecture of the trees with binoculars and by climbing the trees, and chose trees that would allow an experimental design where several boughs could be selected (bough being the main branch attached to the trunk of the tree), and where in each bough we could sample pairs of branches with contrasting light exposure. Other practical aspects to consider were ease of access from the road to transport equipment and the ease and safety of climbing the trees. We finally settled for a *D. guianensis* tree, hereafter named Angela, in the secteur Saint George (4°01'N, 51°59'W), that complied with all our requirements and was fruiting at the moment of sampling. The secteur Saint George experiences an annual rainfall of 3,665 mm and a mean air temperature of 27°C.

The choice of the *Sextonia rubra* individual was dictated by a collaboration with another project, TREE-D, that aims at looking into chemical and holobiont heterogeneity across the whole tree. The tree was just outside of the Paracou Research Station (5°18'N, 52°53'W), and complied with the requirements stated for the *D. guianensis* and was fruiting at the moment of sampling. The Paracou research station experiences an average annual rainfall of 3,041 mm and a mean air temperature of 25.7°C (Aguilos *et al.* 2018).

B - Sampling

We surveyed Sixto on the 13 October 2020 by climbing the tree and selecting suitable boughs that had branches with contrasting light exposure, and then proceeded to sample: 1) Cambium: three cambium tissue samples were collected from the base of the trunk , approximately 1.3m above ground and equidistantly across the perimeter of the tree trunk; 2) Leaves: three leaves from the same twig per branch from eight branches were sampled, the branches were selected in three pairs each in a different bough, plus two independent branches in two other boughs. Branches on boughs were chosen so that each pair of branches contained one light-exposed and one shaded branch, the shade being mostly a result of self-shading (see section C).; and 3) Fruits: fruits were collected from 5 different branches where leaves were collected (Fig. B3). All boughs and branch lengths, and basal and terminal diameters were measured for branches with basal diameters above 10 cm, in addition to the trunk. Sixto was felled on the 14th of October 2020 for analysis of chemical and microbiome heterogeneity across the whole tree for another project, thus the tree is not available for future studies. The sampling of Angela was similar: On 22 April 2021, we

collected: 1) Cambium: three cambium tissue samples were sampled from the base of the trunk of Angela, approximately 1.3m above ground and equidistantly across the perimeter of the tree trunk; 2) Leaves: three leaves from the same twig per branch from ten branches were sampled, the branches were selected as five pairs of branches each in a different bough. Branches on boughs were chosen so that each pair of branches contained one light-exposed and one shaded branch, the shade being mostly a result of self-shading; and, 3) fruits from 4 different branches where leaves were collected (Fig. B4). On 15, 16 and 22 November 2021, we described the architecture of Angela: all branch lengths, and basal and terminal diameters were measured for branches with basal diameters above 10 cm, in addition to the trunk. On 21, 22, and 23 March 2022, 30 wood cores were sampled using a borer across the crown and in the trunk of Angela. Angela was not felled, and is not among the trees planned for felling by the ONF, so it will be accessible for future studies. In both species, leaves,cambium, and fruit samples were flash-frozen in liquid nitrogen and stored at -80ºC until DNA and RNA extraction.

Figure B1: Angela: the Dicorynia guianensis tree sampled in the Régina Saint-Georges forest (4°01'N, 51°59'W).

Figure B2: Sixto: the Sextonia rubra tree sampled near the Paracou research station (5°18'N, 52°53'W).

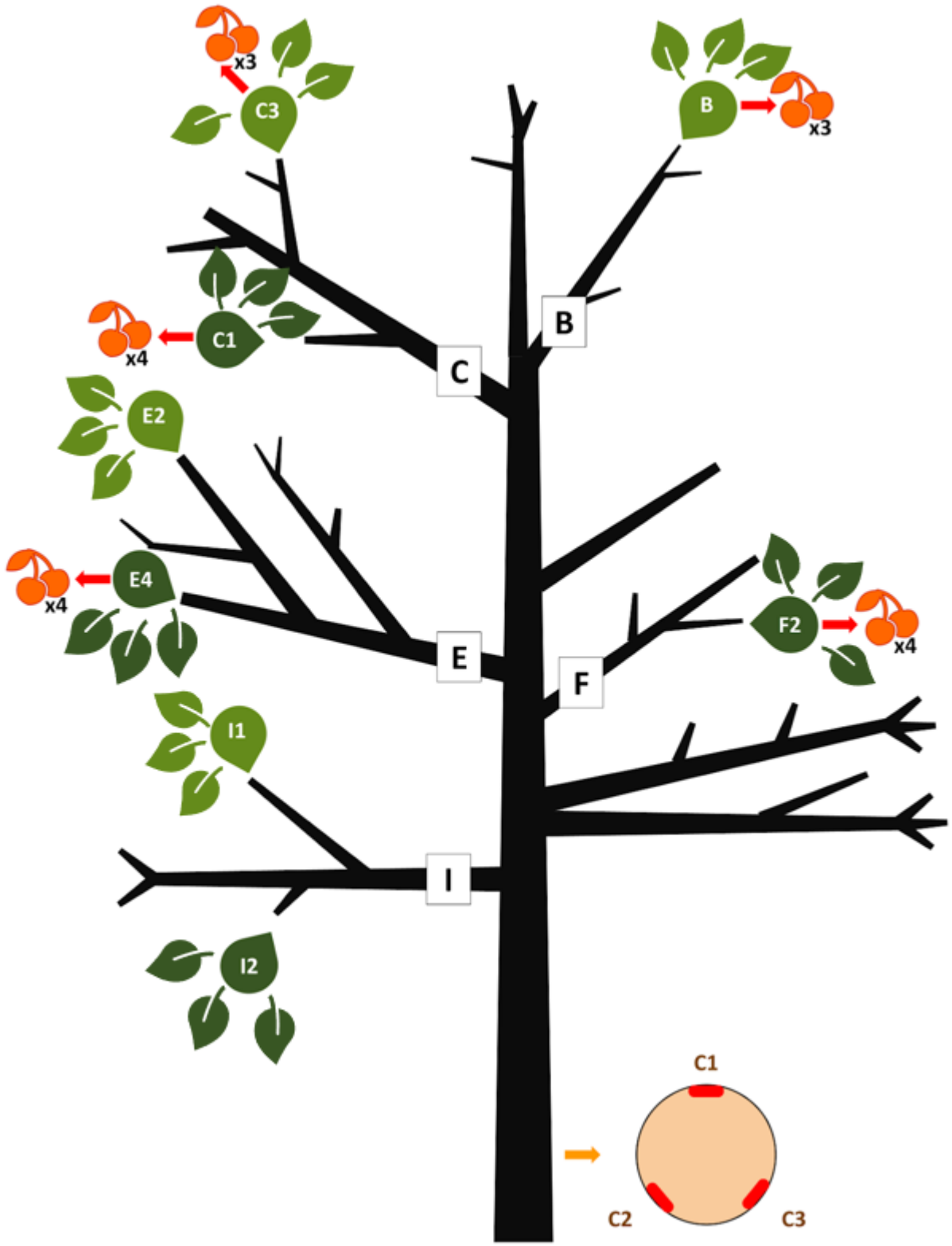

Figure B3: Sixto sampling scheme: Boughs are labelled along the trunk from B to I. The

sampling included (i) three cambium samples from the trunk taken at 1m30 height shown with the salmon-coloured circle facing respectively east, north, and southwest, (ii) three leaves per light condition (light green for light-exposed, dark green for shaded branches) in each pair of branches, and (iii) fruits close to leaf samples B, C1, C3, E4, and F2.

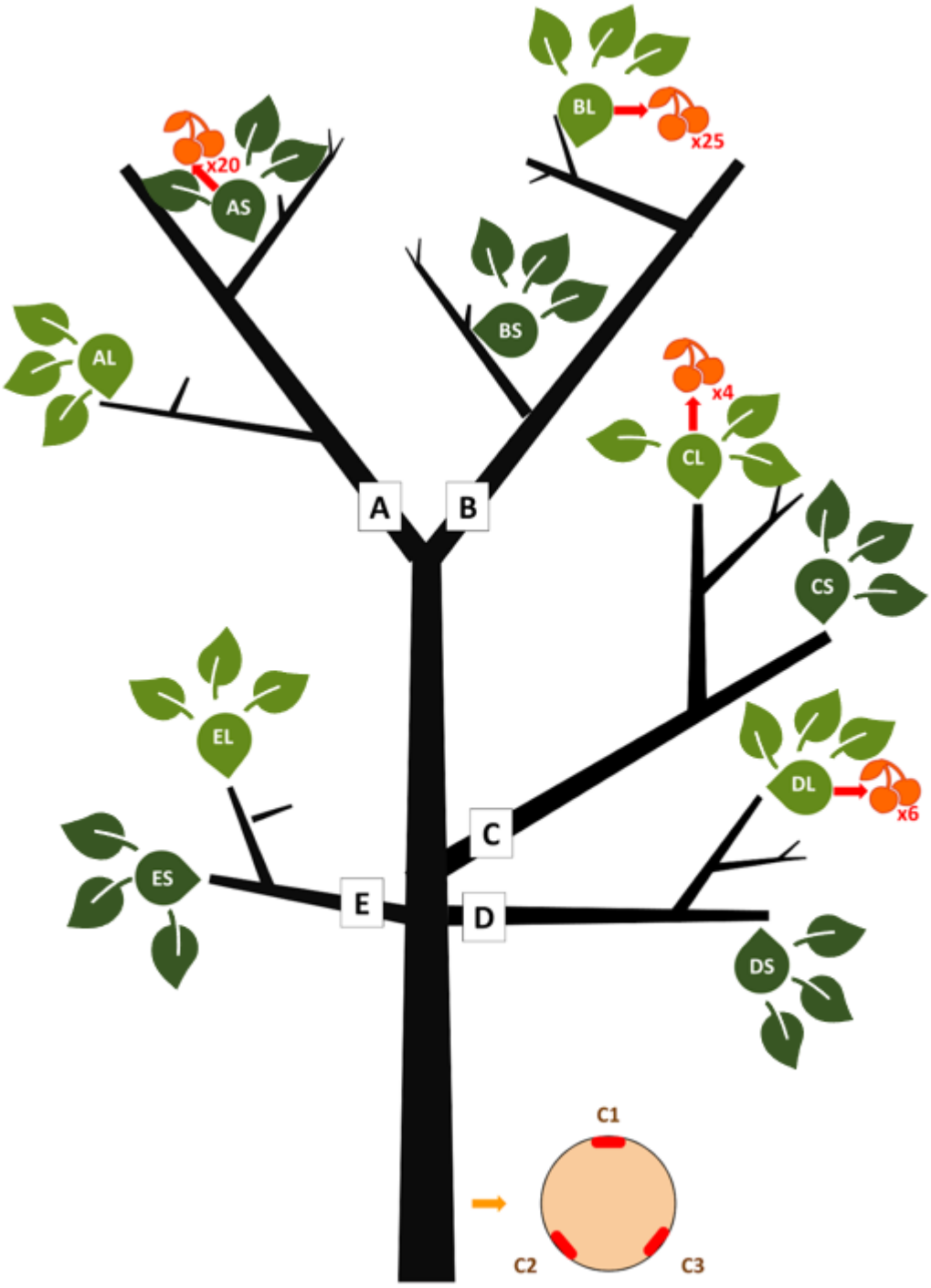

Figure B4: Angela sampling scheme. Boughs are labelled along the trunk from A to E. The sampling included (i) three cambium samples from the trunk taken at 1m30 height shown with the salmon-coloured circle facing respectively east, north, and southwest, (ii) three leaves

per light condition (light green for light-exposed, dark green for shaded branches) in each pair of branches, and (iii) fruits close to leaf samples AS, BL, CL, and DL.

C - Characterisation of light conditions

A linear PAR ceptometer (AccuPar, Decagon Devices, Pullman, WA, USA) was used on each sampling position on both trees during sampling to measure direct incident light around midday in comparison to open incident light measured on the closest road (Tab C1). In addition, for Angela, a terrestrial and drone lidar campaign (TLS, Faro Focus3D 120 ; DLS, Yellowscan Vx20-100) was carried out on 3 May 2021 to map the canopy transmittance in order to derive an estimate of the irradiance in different locations in the canopy. TLS scans were done horizontally from 0-360° and vertically from -60-90° resulting in 174.8 millions of points per scan for 10 scans in a forest gap close to the tree and 4 scans from the nearby road. DLS scans were taken at 35 m above the focal tree in 2 perpendicular flights with flight lines 10 m apart in a circular area 150 m in diameter above the focal tree, resulting in 46.6 million points. Before lidar acquisition, reflective strips were put on sampling points by tree climbers to detect sampling points in the lidar cloud (Fig. C1-A). The AMAPvox software (Vincent *et al.* 2017) was used to compute an annual illumination index from the lidar point cloud. The plant area density (PAD, m2/m3) was calculated for the focal tree in context (with a diameter of 30m surrounding the tree) using 1 m3 voxels. An estimate of the yearly proportion of the above canopy solar radiation received at the sampling point was simulated considering a clearness index of 0.5 and a latitude of 5 degrees. Transmittance uncertainty due to sampling point locations uncertainties was further evaluated by

randomly sampling 10 positions around sampling points up to 0.5 metres (Fig. C1-B) and revealed low variations in transmittance (Table C2). The estimates were in agreement with the light/shade classification of branches identified by the tree climbers (Table C2).

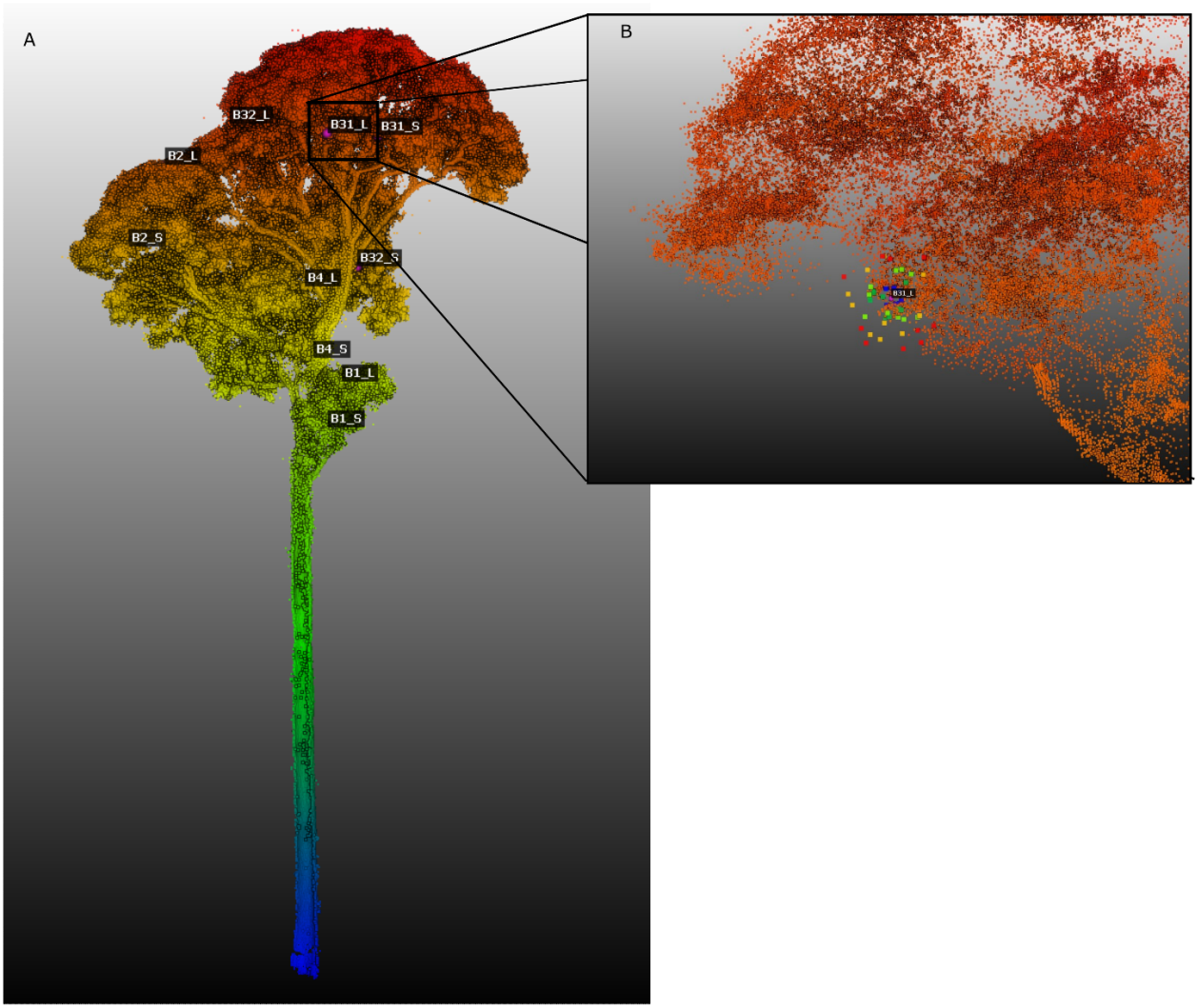

Figure C1: Dicorynia guianensis *lidar point cloud with sampling points. Lidar point cloud was obtained with terrestrial and drone lidar done on the 3rd of May 2021 to characterise annual transmittance. A: the sampling point; B: The random positions from 0.1m (blue) to 0.5m (red)*

every 10cm around the B31 Light sampling point. Refer to table 1 for the correspondence between lidar and genomic IDs.

Table C1: Direct incident light at sampling points in Angela and Sixto: ***branch****: indicates the sampling point as mapped in Fig B3 and Fig B4;* ***PAR****: Photosynthetically active radiation measurement at the sampling point (µmols/m^{2}s);* ***time****: the time the measurement was taken;* ***road****: indicates the PAR measurement at the nearest road (open space), maximum of 100m away from tree.*

	Angela			**Sextonia**	
branch	**PAR** *(µmols/m^{2}s)*	**time**	**branch**	**PAR** *(µmols/m^{2}s)*	**time**
AL	333	14h25	BL	1119	14h46
AS	114	14h10	CL	1036	14h31
BL	192	13h50	CS	91	14h24
BS	88	13h45	EL	1032	14h18
CL	94	15h40	ES	169	14h00
CS	94	15h45	FS	56	13h56
DL	150	13h40	IL	1170	13h45
DS	83	13h30	IS	47	13h30
EL	160	15h00			
ES	88	15h03			
Road	305	15h10	**Road**	1860	13h25

Table C2: Radiation balance at the ten sampling points in Angela. Table C2 summarises lidar and genomic identifiers for branches with corresponding light condition assessed by climbers and the transmittance estimated from the radiation balance. The standard deviation of transmittance in parenthesis is given for a distance of 0.5m from the identified sampling point.

ID lidar	ID genomic	Condition	Transmittance (standard deviation)	Height above ground
B31	AL	light	0.34 (0.09)	44.31
B31	AS	shadow	0.08 (0.02)	44.76
B32	BL	light	0.84 (0.22)	46.44.7
B32	BS	shadow	0.15 (0.04)	38.08
B4	CL	light	0.17 (0.04)	37.18
B4	CS	shadow	0.08 (0.02)	33.6
B2	DL	light	0.80 (0.08)	43.25
B2	DS	shadow	0.16 (0.04)	38.95
B1	EL	light	0.43 (0.01)	31.45
B1	ES	shadow	0.09 (0.04)	28.97

D - Genome assemblies and annotations

High molecular weight (HMW) DNA was extracted from 2g of frozen leaves using QIAGEN Genomic-tips 500/G kit (Qiagen, MD, USA). We have followed the tissue protocol extraction. Briefly, 2g of young leaf material were grounded in liquid nitrogen with mortar and pestle. After 3h of lysis and one centrifugation step, the DNA was immobilised on the column. After several washing steps, DNA is eluted from the column, then desalted and concentrated by Isopropyl alcohol precipitation. A final wash is done with 70% ethanol before resuspending the DNA in the EB buffer. DNA quantity and quality were assessed with NanoDrop and Qubit (Thermo Fisher Scientific , MA, USA). DNA integrity was also assessed using the Agilent FP-1002 Genomic DNA 165 kb on the Femto Pulse system (Agilent, CA, USA). Hifi libraries were constructed using SMRTbell® Template Prep kit 2.0 (Pacific Biosciences, Menlo Park, CA, USA) according to PacBio recommendations (SMRTbell® express template prep kit 2.0 - PN: 100-938-900). HMW DNA samples are first purified with 1X Agencourt AMPure XP beads (Beckman Coulter, Inc, CA USA), and sheared with Megaruptor 3 (Diagenode, Liège, BELGIUM) at an average size of 20 kb. After End repair, A-tailing and ligation of SMRTbell adapter, the library is size selected on BluePippin System (Sage Science, MA,USA) at range size of 10-50kb. The size and concentration of libraries were assessed using the Agilent FP-1002 Genomic DNA 165 kb on the Femto Pulse system and the Qubit dsDNA HS reagents Assay kit. Sequencing primer v5 and Sequel® II DNA Polymerase 2.2 were annealed and bound, respectively, to the SMRTbell libraries. Each library was loaded on 2 SMRTcell 8M at an on-plate concentration of 90pM. Sequencing was performed on the Sequel® II system at Gentyane Genomic Platform (INRAE Clermont-Ferrand, France) with

Sequel® II Sequencing kit 3.0, a run movie time of 30 hours with an Adaptive Loading target (P1 + P2) at 0.75. We obtained 1,898,004 corrected reads for *D. guianensis* (N50=21,233; DP=58.7X), that we assembled in 562 contigs (N50=37.76Mb; L50=8 contigs; GC=37.25%) using *HiFiasm assembler* (v0.15.5, Cheng *et al.*, 2021). *Hifiasm* is able to produce 2 haplotype aware assemblies where the alleles are separated in two files. All the metrics correspond to the haplotype1 file and only this one was used for the next analysis. Similarly, we obtained 6,624,997 corrected reads for *S. rubra* (N50=17,577; DP=114X), that we assembled in 747 contigs (N50=16.513Mb; L50=17 contigs; GC=38.50%).

HMW DNA was additionally used to produce optical maps for hybrid scaffolding. The HMW DNA was labelled and stained according to the Direct Label and Stain (DLS) protocol (BNG). Briefly, labelling was achieved by incubating 750 ng genomic DNA with 1× DLE-1 Enzyme (BNG) for 2 hours in the presence of 1× DL-Green (BNG) and 1× DLE-1 Buffer (BNG). Following proteinase K digestion and DL-Green clean-up, the DNA backbone was stained by mixing the labelled DNA with DNA Stain solution (BNG) in the presence of 1×Flow Buffer (BNG) and 1× DTT (BNG), and incubating overnight at room temperature. The DLS DNA concentration was measured with the Qubit dsDNA HS Assay (Invitrogen, Carlsbad, CA, USA). Labelled and stained DNA was loaded on 1 Saphyr chip for each species. The chips were loaded and run on the BNG Saphyr System according to the Saphyr System User Guide. Digitalised labelled DNA molecules were assembled to optical maps using the BNG Access software. A total of 972 Gb (*D. guianensis*) and 720 Gb (*S. rubra*) of molecules with a size larger than 150kb, the threshold for map assembly, were generated representing 1,500x and 720X of genome coverage, respectively. The *D. guianensis* assembly produced

511 genome maps with a N50 of 15.7 Mb for a total genome map length of 903 Mbp. The *S. rubra* assembly produced 314 genome maps with a N50 of 14,95 Mb for a total genome map length of 1329 Mbp. Finally, a hybrid scaffolding was assembled between the sequence assembly and the optical genome maps with hybridScaffold pipeline (https://bionano.com/wp-content/uploads/2023/01/30073-Bionano-Solve-Theory-of-Operation-Hybrid-Scaffold.pdf). For *D. guianensis*, we obtained 54 hybrid scaffolds (N50=38.450Mb; N=0.76%; 571 gaps), while 515 contigs remained unanchored with a total length of 28,784Mb representing 4.97% of the genome. For *S. rubra*, we obtained 35 hybrid scaffolds (N50=60.458Mb; N=1%; 1,923 gaps), while 609 contigs remained unanchored with a total length of 53,067Mb representing 5.08% of the genome.

We built an automated workflow for genome annotation named *genomeAnnotation* (see script availability). We used both *singularity* containers (Kurtzer *et al.,* 2017) and the *snakemake* workflow engines (Köster *et al.,* 2012) to make the workflow highly reproducible (FAIR), and scalable. The workflow accomplishes: (i) *de novo* and known transposable element (TE) detection, (ii) *de novo* and known gene models detection, and (ii) gene functional annotation. *De novo* TE detection uses *RepeatModeler2* (v2.0.3; Flynn *et al.*, 2020) followed by classification using *RepeatClassifier* (v2.0.3; Flynn *et al.*, 2020) and *TEclass* (v2.1.3; Abrusán *et al.*, 2009). The obtained *de novo* TE are merged with known TE accessions for *Viridiplantae* from *RepBase* (v27.07; Kapitonov and Jurka 2008). This consolidated database is used for TE detection in each genome before soft masking using *RepeatMasker* (v2.0.3; Flynn *et al.*, 2020). *De novo* and known gene models detection rely on *BRAKER2* and its dependencies (Brůna *et al.*, 2020). Finally, functional annotation of

candidate genes is based on the *Trinotate* pipeline (v3.2.1; Bryant *et al.*, 2017) using *TransDecoder* (v5.5.0; https://github.com/TransDecoder/TransDecoder), *TMHMM* (Krogh *et al.*, 2001), *HMMER* (Finn *et al.*, 2011), *BLAST* (v2.13.0; Altschul *et al.*, 1990), *RNAmmer* (v1.2; Lagesen *et al.*, 2007), and *SignalP* (v4.1; Petersen *et al.*, 2011) with *UniProt* (Bateman *et al.*, 2015) and *Pfam* databases (Punta *et al.*, 2012).

Two high quality genomes were obtained for *Dicorynia guianensis* and *Sextonia rubra* with a total length of 550 and 991 Mb and 54 and 35 super-scaffolds anchored with optical maps, respectively, including 20 super-scaffolds > 1 Mb in each species. Evaluation of completeness for the two assemblies was done with BUSCO (Seppey *e al.,* 2019), revealing near complete assemblies (>99% of the *Viridiplantae* housekeeping genes, 352 and 409 complete single-copy genes for *Dicorynia guianensis* and *Sextonia rubra,* respectively, Fig. D1). Genome heterozygosity (π) was estimated based on K-mer distributions and was found to be 0.9% and 0.7% for *Dicorynia guianensis* and *Sextonia rubra,* respectively (Fig. D2 & D3). Consistent with the smaller genome size of *D. guianensis*, we detected fewer genes (15,490) and a lower transposable elements content (50.8%) in *D. guianensis* as compared to *S. rubra* (21,412 and 63.8%, respectively). Genomic distributions of TE were highly heterogeneous across super-scaffolds (Fig. D4 & Fig. D5). TE annotations revealed a majority of long terminal repeat elements (16%-23.3%) and DNA transposons (3.4%-16%, Fig. D6 & Fig. D7).

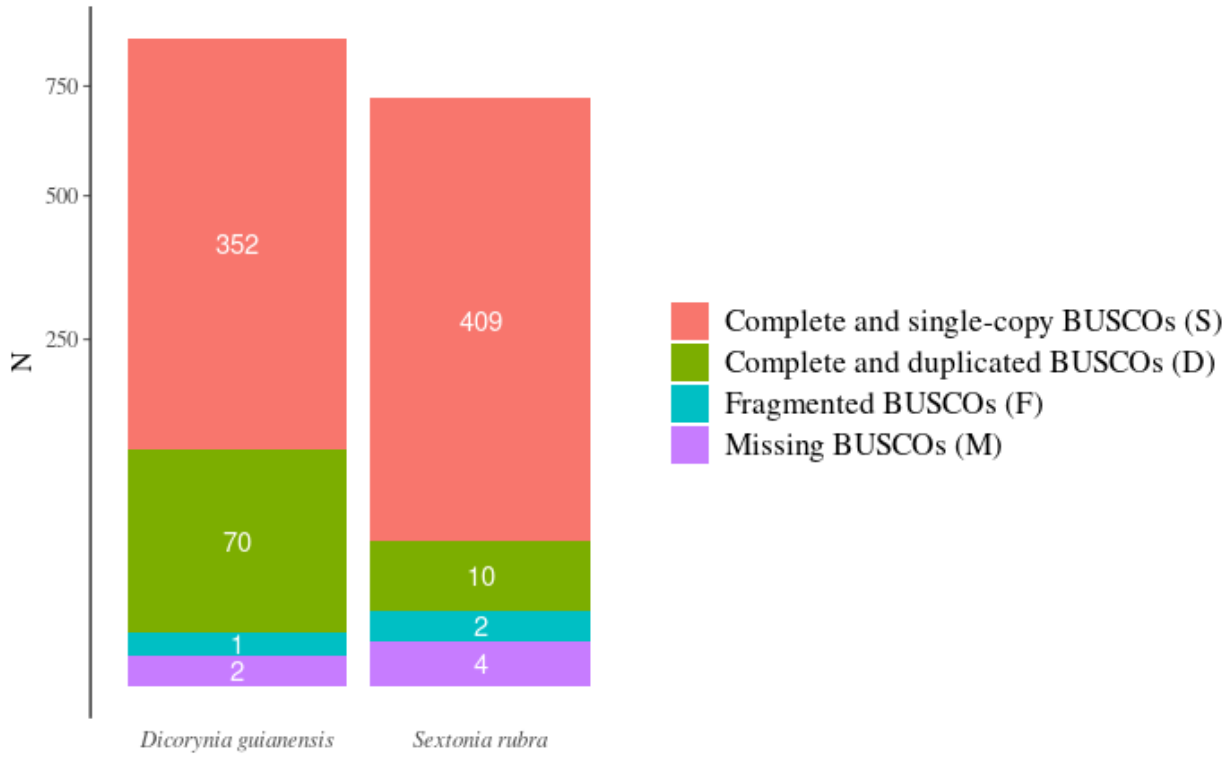

Figure D1: Dicorynia guianensis *and* Sextonia rubra *genome completeness assessed by BUSCO analyses (Seppey e al., 2019) with Viridiplantae housekeeping genes.*

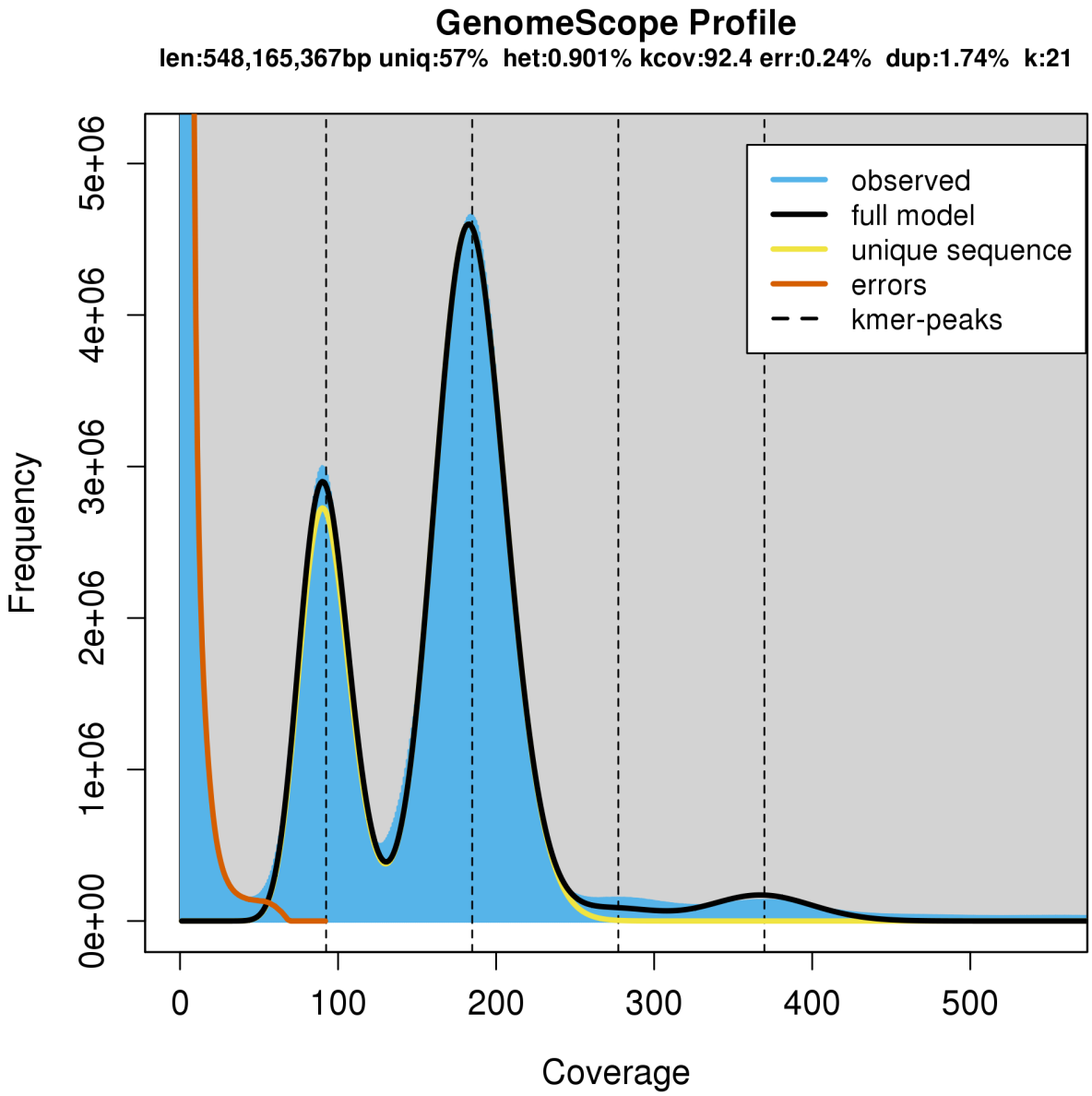

Figure D2: Dicorynia guianensis *heterozygosity estimated at 0.901% with a K-mer based method using Jellyfish (v1.1.12; Marçais and Kingsford 2011) and the GenomeScope (Vurture et al., 2017) with up to 21-mer.*

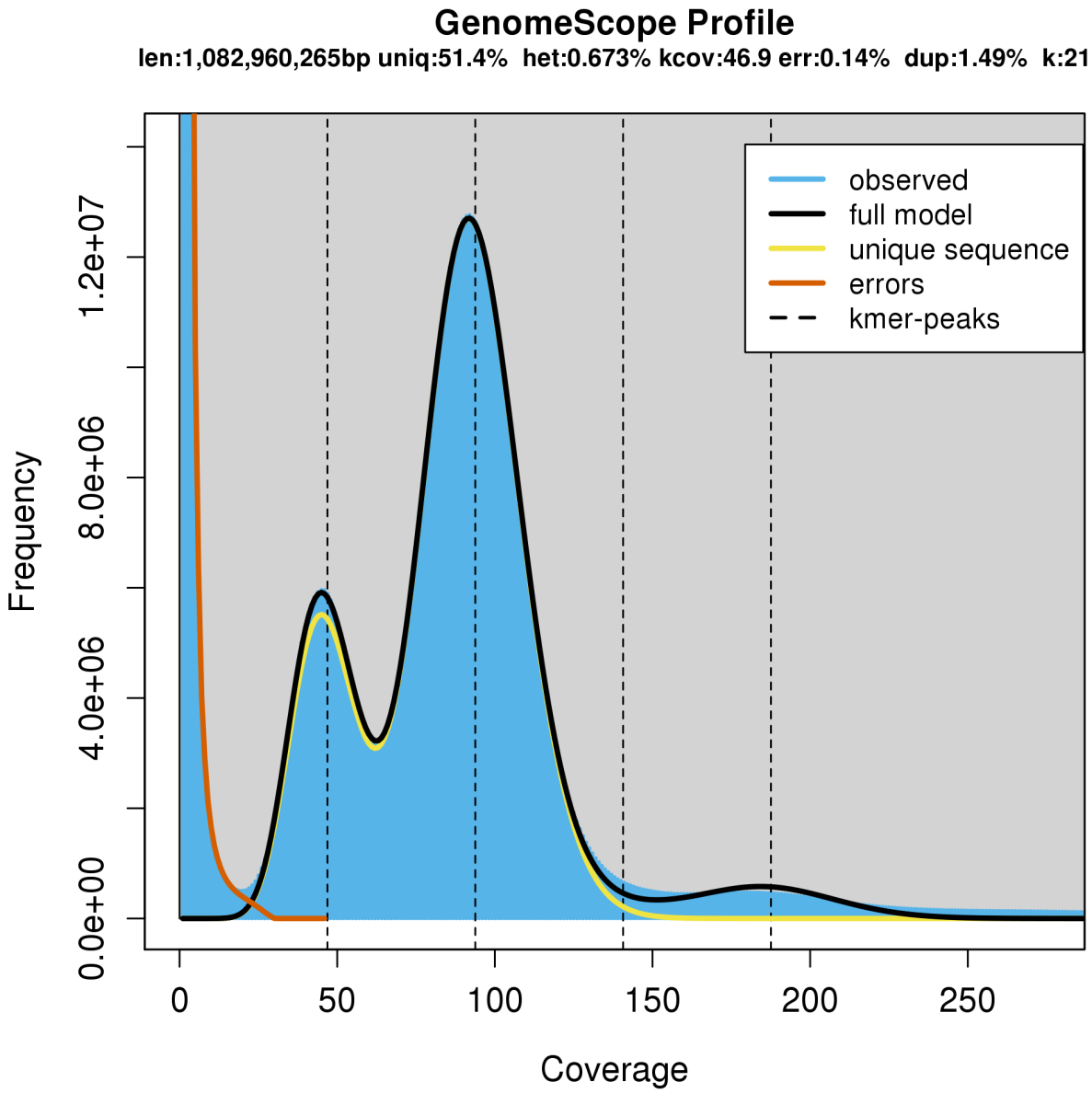

Figure D3: Sextonia rubra *heterozygosity estimated at 0.673% with a K-mer based method using Jellyfish (v1.1.12; Marçais and Kingsford 2011) and the GenomeScope (Vurture et al., 2017) with up to 21-mer.*

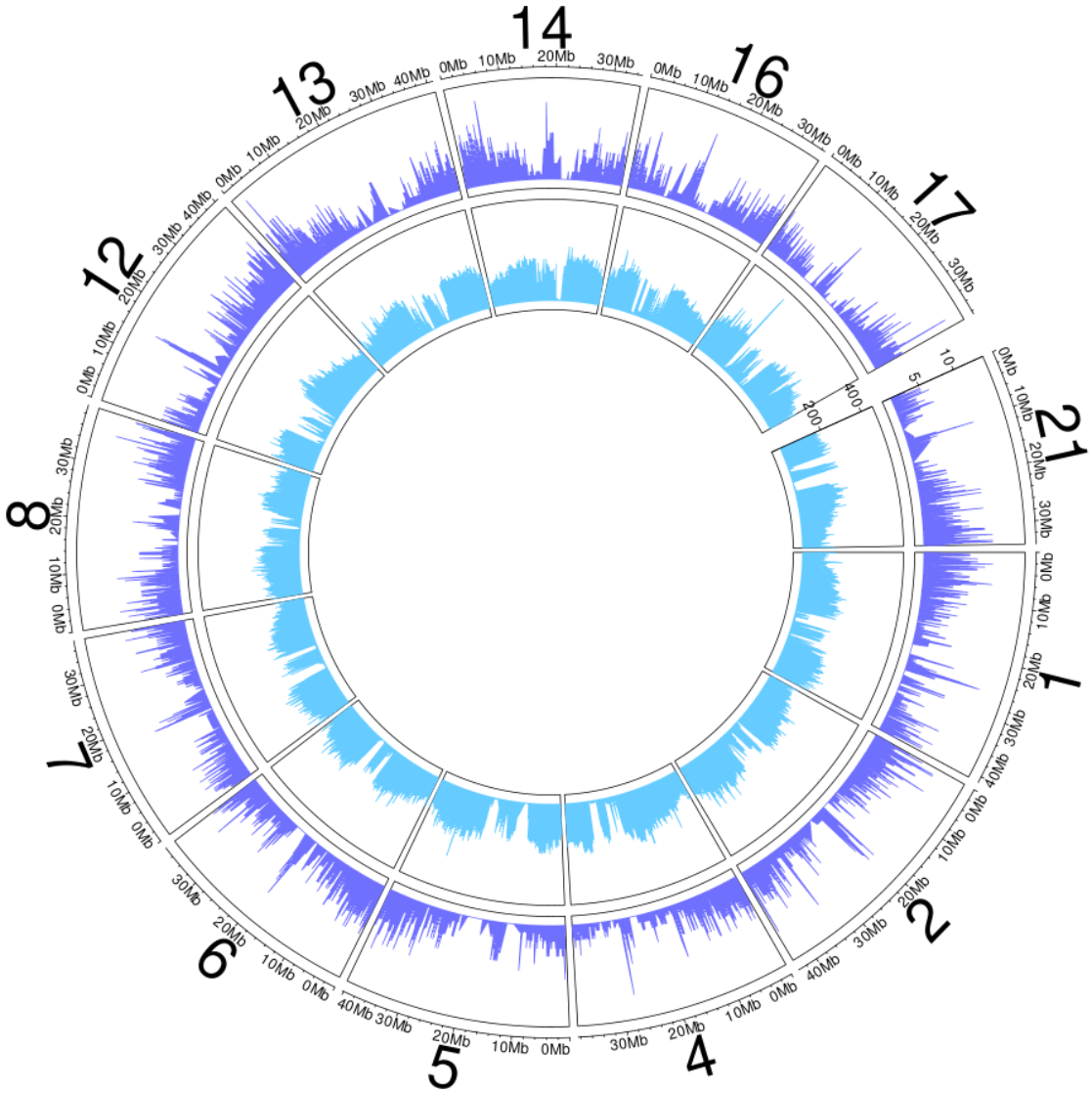

Figure D4: Transposable elements (TE) and gene distribution across the genome of Dicorynia guianensis *on a 0.1MB sliding window. The outer circle shows genes count in purple, and the inner circle shows TE count blue. Number indicates super-scaffolds id. Only scaffolds with a length above 20Mb are shown.*

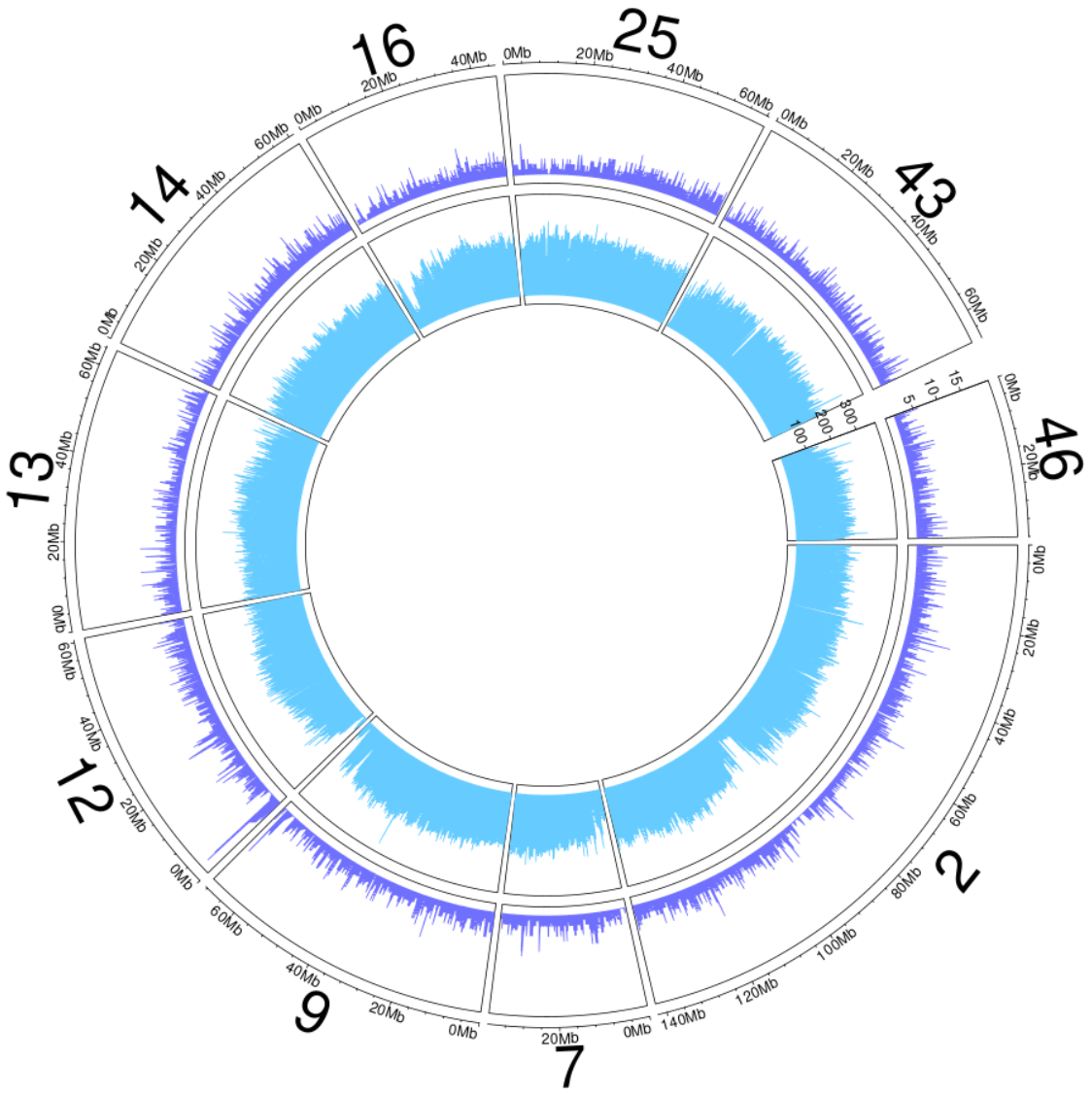

Figure D5: Transposable elements (TE) and gene distribution across the genome of Sextonia rubra*. on a 0.1MB sliding window. The outer circle shows genes count in purple, and the inner circle shows TE count blue. Number indicates super-scaffolds id. Only scaffolds with a length above 35Mb are shown.*

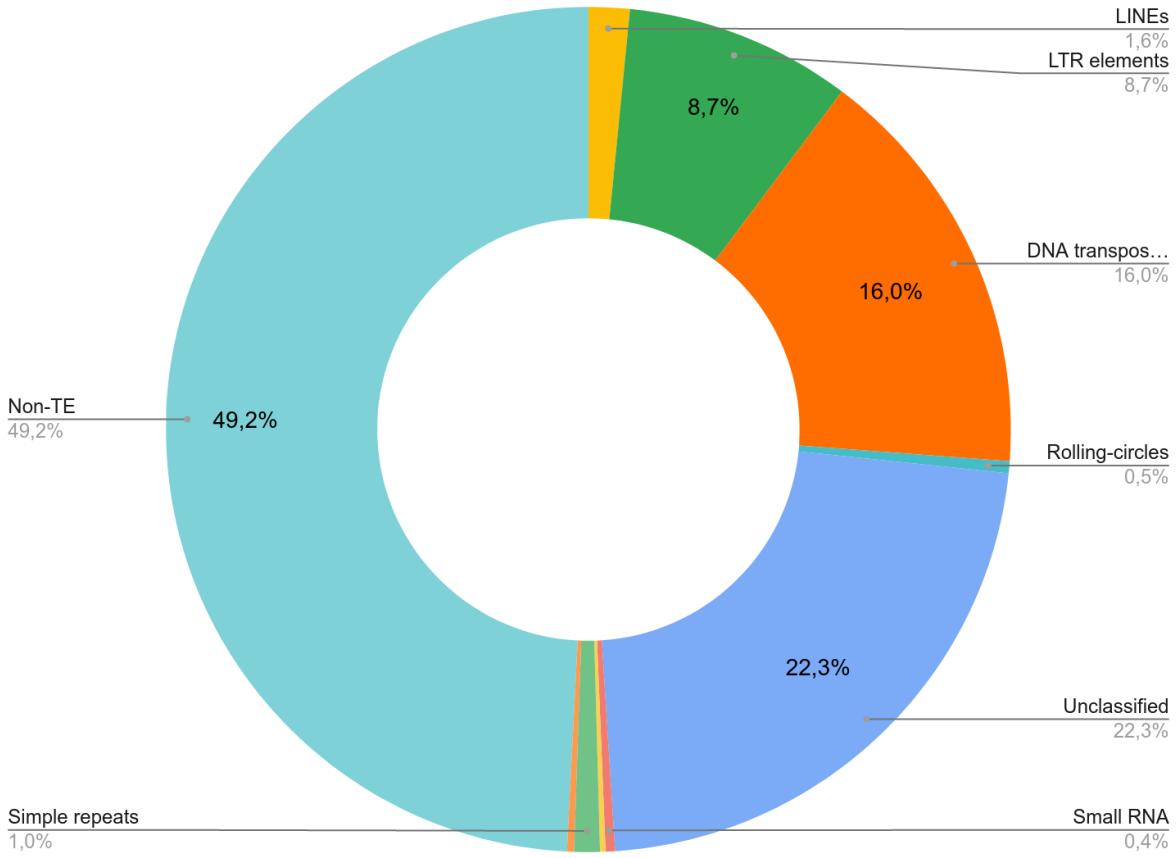

Figure D6: Transposable elements (TE) annotation for Dicorynia guianensis*. Percentage of genome total length in non-TE, low-complexity DNA, repeats, satellites, small RNA, unclassified TE, rolling circles, DNA transposons, long terminal repeats (LTR) elements, and long interspersed nuclear elements (LINEs). De novo detection of TE resulted in 22.3% of unclassified TE by RepeatClassifier.*

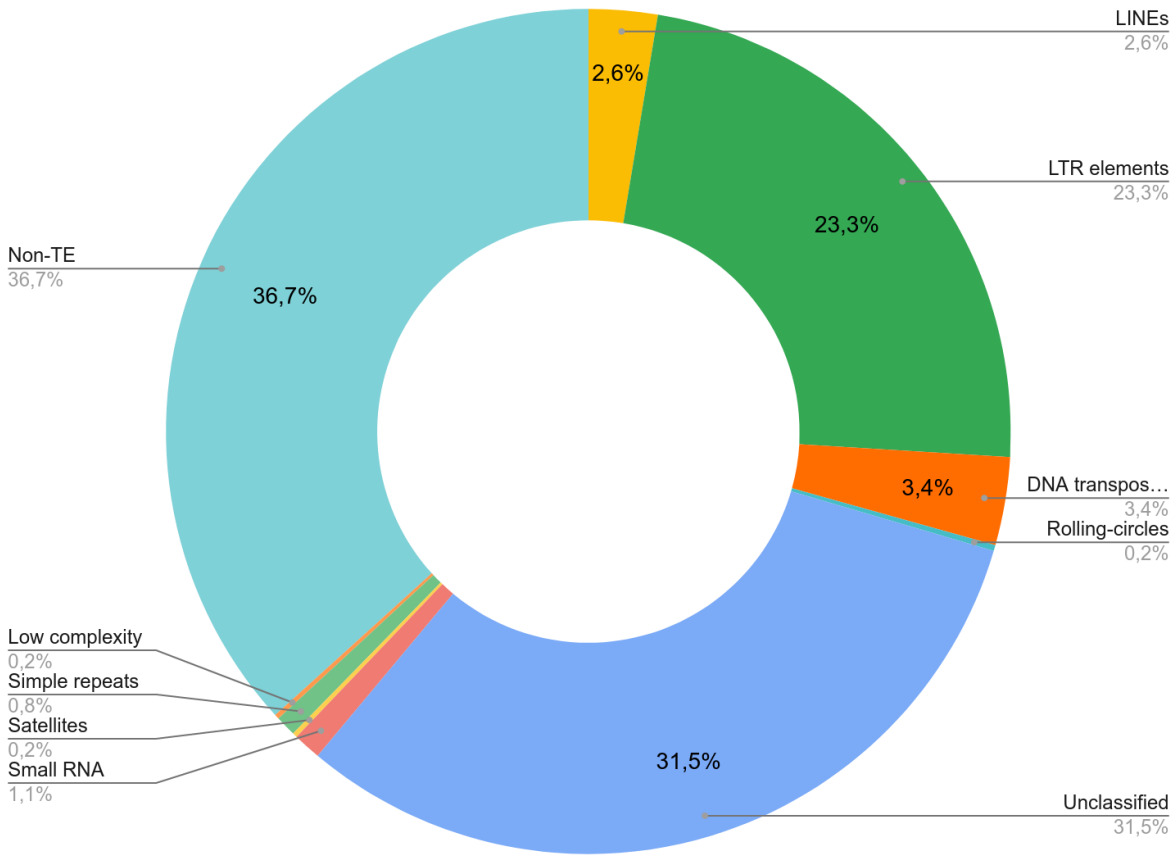

Figure D7: Transposable elements (TE) annotation for Sextonia rubra*. Percentage of genome total length in non-TE, low-complexity DNA, repeats, satellites, small RNA, unclassified TE, rolling circles, DNA transposons, long terminal repeats (LTR) elements, and long interspersed nuclear elements (LINEs). De novo detection of TE resulted in 22.3% of unclassified TE by RepeatClassifier.*

E - Leaf and cambium mutation detection

Genomic DNA was extracted from 30 mg of frozen leaf or cambium tissue per sampling point for both trees with a CTAB protocol with chloroform - isoamyl alcohol (24:1) extraction, isopropanol precipitation and pellet resuspension in 1x Low TE (10 mM Tris-HCl + 0.1 mM EDTA; Doyle and Doyle 1987). DNA was quantified using a Qubit HS assay (Thermo Fisher Scientific, Waltham, MA, USA) and purified with AMPure XP beads (Beckman Coulter Genomics, Danvers, MA, USA) when required to allow library preparation. An Illumina sequencing library was produced for each leaf using an optimised NEBNext Ultra II DNA library protocol (New England Biolabs, Ipswich, MA, USA). Libraries were pooled in multiplexes after tagging each library independently before whole genome sequencing (WGS) on a S4 flow cell and in a NovaSeq 6000 instrument with v1.5 chemistry (2 x 150 PE mode). We obtained 33 cambium and leaf libraries for Angela with a sequencing depth of about 160X and 27 libraries with a depth of about 80X for Sixto (Fig. E1).

We built a workflow to detect somatic mutations from mapped sequencing reads on a genome reference named *detectMutations* (see script availability and Schmitt *et al.*, 2022). S*ingularity* containers (Kurtzer *et al.,* 2017) and the *snakemake* workflow engines (Köster *et al.,* 2012) were used to ensure an automated, highly reproducible (FAIR), and scalable workflow. Pair-end sequencing reads of every library are quality checked using *FastQC* (v0.11.9) before trimming using *Trimmomatic* (v0.39, Bolger *et al.,* 2014) keeping only paired-end reads without adaptors and a phred score above 15 in a sliding window of 4 bases. Reads are aligned against the reference genome using BWA *mem* with the option to

mark shorter splits (v0.7.17, Li & Durbin, 2009). Alignments are then compressed using *Samtools view* in CRAM format, sorted by coordinates using *Samtools sort,* and indexed using *Samtools index* (v1.10, Li *et al.,* 2009). Duplicated reads in alignments are marked using *GATK MarkDuplicates* (v4.2.6.1, Auwera *et al.,* 2013). Sequencing depth is estimated along the genome using *Mosdepth* (v0.2.4, Pedersen *et al.,* 2018) globally and on a 1-kb sliding window.

We used both a K-mer based and an alignment based method to estimate heterozygosity and detect heterozygous sites. We used *Jellyfish* (v1.1.12; Marçais and Kingsford 2011) and *GenomeScope* (Vurture *et al.,* 2017) to estimate heterozygosity up to 21-mer. We used *GATK (HaplotypeCaller, GatherGVCFs, GenomicsDBImport, GenotypeGVCFs;* Auwera *et al.,* 2013) to call heterozygous sites from previously obtained alignments. We filtered single nucleotide polymorphisms (SNP) using *bcftools* (v1.10.2, Danecek *et al.,* 2021), *GATK VariantFiltration* (v4.2.6.1, Auwera *et al.,* 2013), and *plink* (v1.90, Chen *et al.,* 2019). To filter candidate variants, we kept only biallelic SNPs with a quality below 30, a quality by depth below 2, a Fisher strand ratio above 60 and a strand odds ratio above 3. To remove all sites that were truly heterozygous, we further filtered SNPs present in all genotypes and sampled tissues (no missing data) and shared by at least all tissues but one. Finally, the workflow uses *Strelka2* (v2.9.10, Kim *et al.,* 2018) to detect mutations, a variant caller developed initially for cancer research. This software has been shown to perform best in our study design (Schmitt *et al.*, 2022). *Strelka2* identifies mutations by comparing two samples, one mutated and one normal sample (directional). To detect cambium mutations present at the base of the tree we compared all potential pairs (6 in total) among the three cambium libraries. To

detect leaf mutations we called each leaf library against the first cambium library (T2 for Anglea and T1 for Sixto) as the reference sample. We filtered from leaf candidate mutations previously identified heterozygous sites and all candidate mutations from all the cambium comparisons using *BEDTools subtract* (v2.29.2, Quinlan & Hall, 2010). We further filtered mutations using the following criteria: (i) no copy of the mutated allele in the reference sample being here the cambium sample; (ii) a read depth for the two samples between the 5th quantile and the 95th quantile of the coverage of the corresponding library; and (iii) the presence of the mutation in at least two biological replicates (at least 2 leaves from the crown). We produced two datasets with the filtered mutations: (i) all filtered mutations; and (ii) a more stringent dataset that passed the empirical variant score (EVS) filtering of *Strelka2* (v2.9.10, Kim *et al.,* 2018). We used the same pipeline and compared detected mutations on two pedunculate oaks *Quercus robur* (Schmitt *et al.*, 2022) named Napoleon (Schmid-Siegert *et al.* 2017) and 3P (Plomion *et al.* 2018), and on an unpublished dataset from one tortuous beech *Fagus sylvatica* (C. Plomion pers. com.). We detected a total of 15,066 unique somatic mutations in Angela and 3,208 in Sixto by comparison with the cambium reference samples. Similarly, we found 2,356 and 13,976 unique somatic mutations in Napoleon and 3P, respectively, and 6,560 unique somatic mutations in the tortuous beech.

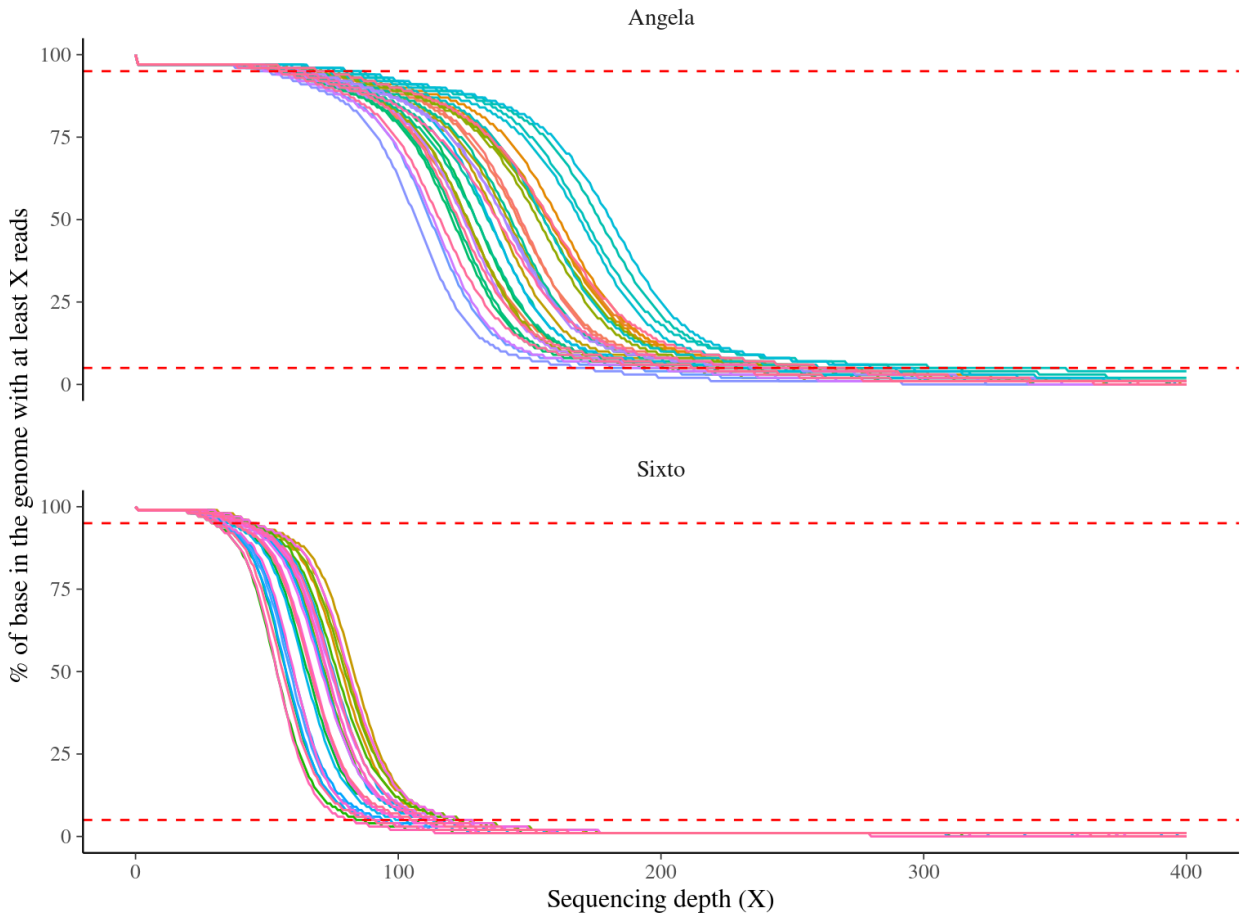

Figure E1: Sequencing depth for Angela and Sixto libraries (cambium and leaves). The x-axis shows the sequencing depth while the y-axis shows the percentage of bases with at least the corresponding sequencing depth. Metrics were calculated over sliding windows of 1 kb.

F - Mutations along the tree architecture

We explored mutation distribution along tree architecture by assuming the origin of the mutation in the tree architecture was at the latest the most recent common branching event among all branches harbouring the mutation (Duan *et al.,* 2022). Among the 15,066 and

3,208 unique somatic mutations identified in Angela and in Sixto, respectively, 10,849 (72.0%) and 1,381 (43.0%) of the mutations originated at the latest from the base of the crown, a proportion far more important than from the tips (824 (5.5%) and 283 (8.8%) respectively; Fig. F1). Nevertheless most mutations were only weakly shared among sampling points, *i.e.* only by a few branches among all branches in common (Fig. F2 & Fig. F3), resulting in low correlations among sampling points (Tab. F1 & Tab. F2). We further built mutation phylogenies using *iqtree* rooting the tree with the non-mutated library from the cambium mean genotype without mutations (Nguyen *et al.,* 2015), and found very divergent sampling points in both individuals with low support for the tree topology (Fig. F4). We compared phylogenies to the physical architecture of both trees with the *dendextend* R package (Galili 2015). Contrary to the general expectation in plants, the observed phylogeny at the somatic mutation positions do not follow the tree architecture, neither in Angela nor Sixto (Fig. F5 and Fig. F6).

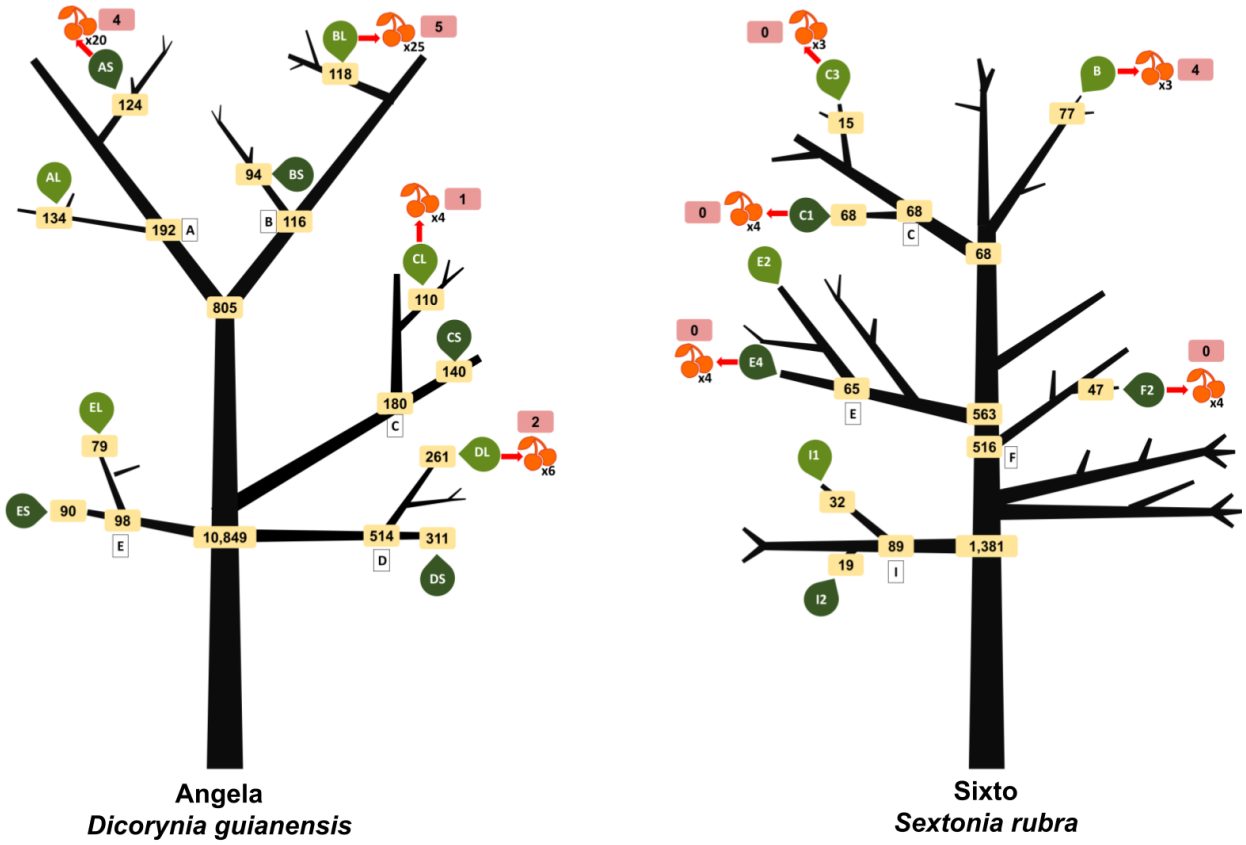

Figure F1: Origin of mutations in the crown of Angela and Sixto. After filtering out mutations with a minimum of 5 copies, no copies in the reference sample, a sequencing depth between the 5th and 95th quantile of the corresponding library and present in at least two samples in the crown, we classified their origin as the most recent branching event of the shared mutation by all samples carrying it. Numbers in yellow boxes give the corresponding number of mutations originating from this branching event.

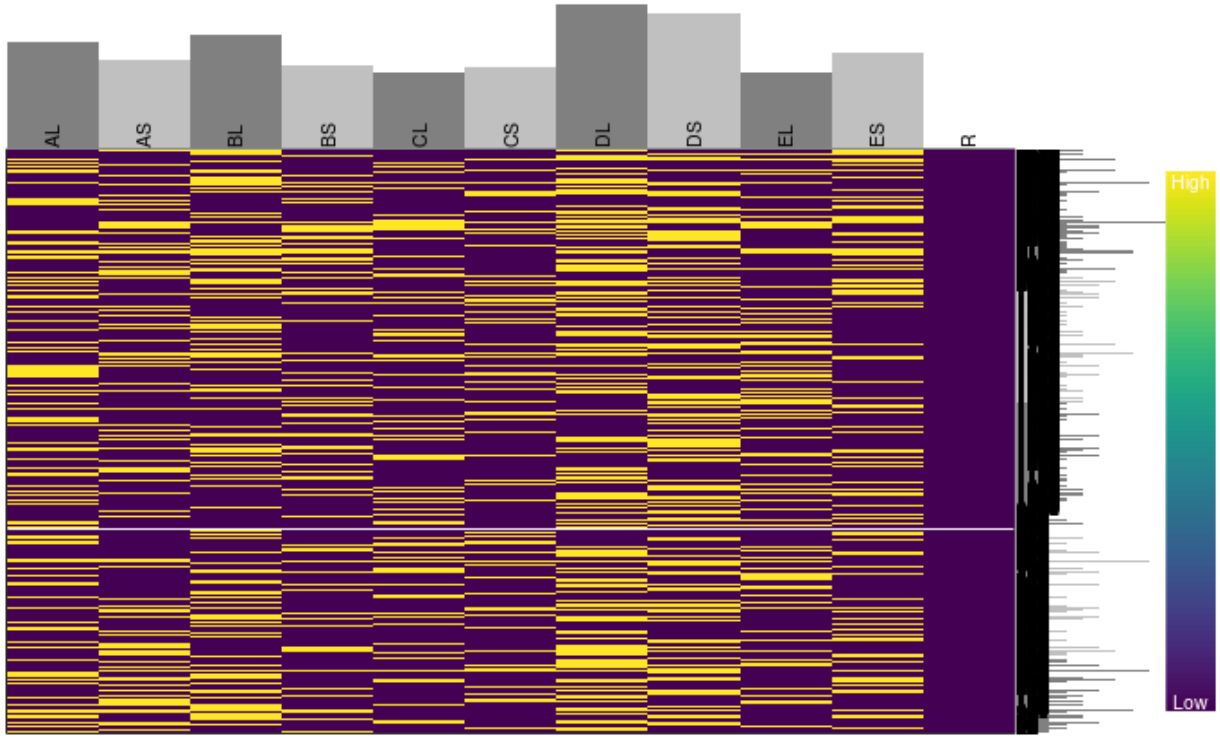

Figure F2: Heat map of somatic mutations on super-scaffold 1 in Angela (lines) in each sample point (lines) with bar graphs representing the total number of accumulated mutations. Yellow represents mutations while purple represents the ancestral state with R representing the fully ancestral root.

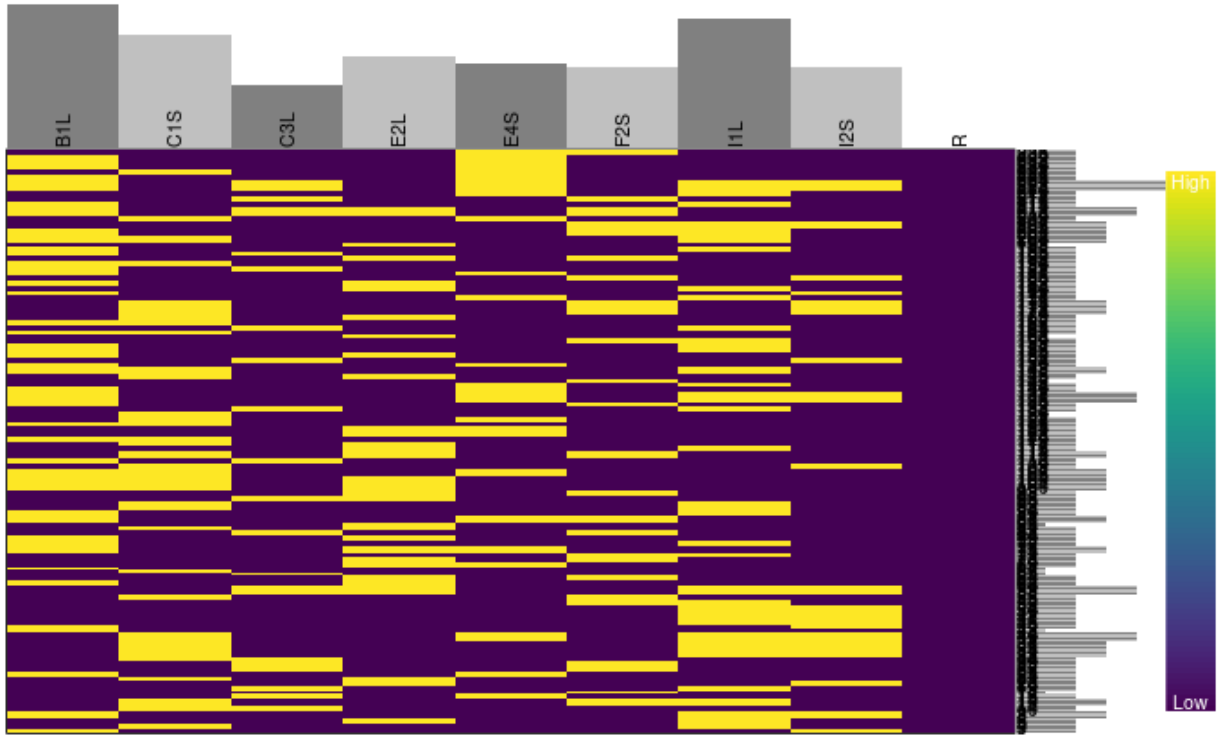

Figure F3: Heat map of somatic mutations on super-scaffold 10 in Sixto (lines) in each sample point (columns) with bar graphs representing the total number of accumulated mutations. Yellow represents mutations while purple represents the ancestral state with R representing the fully ancestral root.

Table F1: Correlations of Angela mutations among sample point pairs. See figure F1 for labels.

	AL	AS	BL	BS	CL	CS	DL	DS	EL	ES
AL	1.00	0.01	-0.02	0.01	0.00	0.02	-0.05	-0.03	-0.01	0.00
AS	0.01	1.00	-0.03	0.09	-0.01	-0.04	0.07	-0.04	-0.01	-0.01
BL	-0.02	-0.03	1.00	-0.03	0.01	-0.02	-0.02	-0.02	-0.03	0.04
BS	0.01	0.09	-0.03	1.00	0.01	-0.01	0.03	-0.03	0.00	0.00
CL	0.00	-0.01	0.01	0.01	1.00	0.01	-0.05	-0.03	-0.01	-0.05
CS	0.02	-0.04	-0.02	-0.01	0.01	1.00	-0.03	-0.01	0.02	0.00
DL	-0.05	0.07	-0.02	0.03	-0.05	-0.03	1.00	-0.07	0.00	0.02
DS	-0.03	-0.04	-0.02	-0.03	-0.03	-0.01	-0.07	1.00	-0.02	0.00
EL	-0.01	-0.01	-0.03	0.00	-0.01	0.02	0.00	-0.02	1.00	-0.02
ES	0.00	-0.01	0.04	0.00	-0.05	0.00	0.02	0.00	-0.02	1.00

Table F2: Correlations of Sixto mutations among sample point pairs. See figure F1 for labels.

	B1L	C1S	C3L	E2L	E4S	F2S	I1L	I1S
B1L	1.00	-0.09	-0.05	-0.08	-0.02	-0.07	-0.05	-0.05
C1S	-0.09	1.00	-0.06	-0.05	-0.02	-0.05	-0.06	-0.03
C3L	-0.05	-0.06	1.00	-0.03	-0.01	-0.03	-0.06	-0.01
E2L	-0.08	-0.05	-0.03	1.00	-0.04	-0.07	-0.05	-0.03
E4S	-0.02	-0.02	-0.01	-0.04	1.00	-0.02	-0.06	-0.04
F2S	-0.07	-0.05	-0.03	-0.07	-0.02	1.00	-0.07	-0.06
I1L	-0.05	-0.06	-0.06	-0.05	-0.06	-0.07	1.00	-0.02
I2S	-0.05	-0.03	-0.01	-0.03	-0.04	-0.06	-0.02	1.00

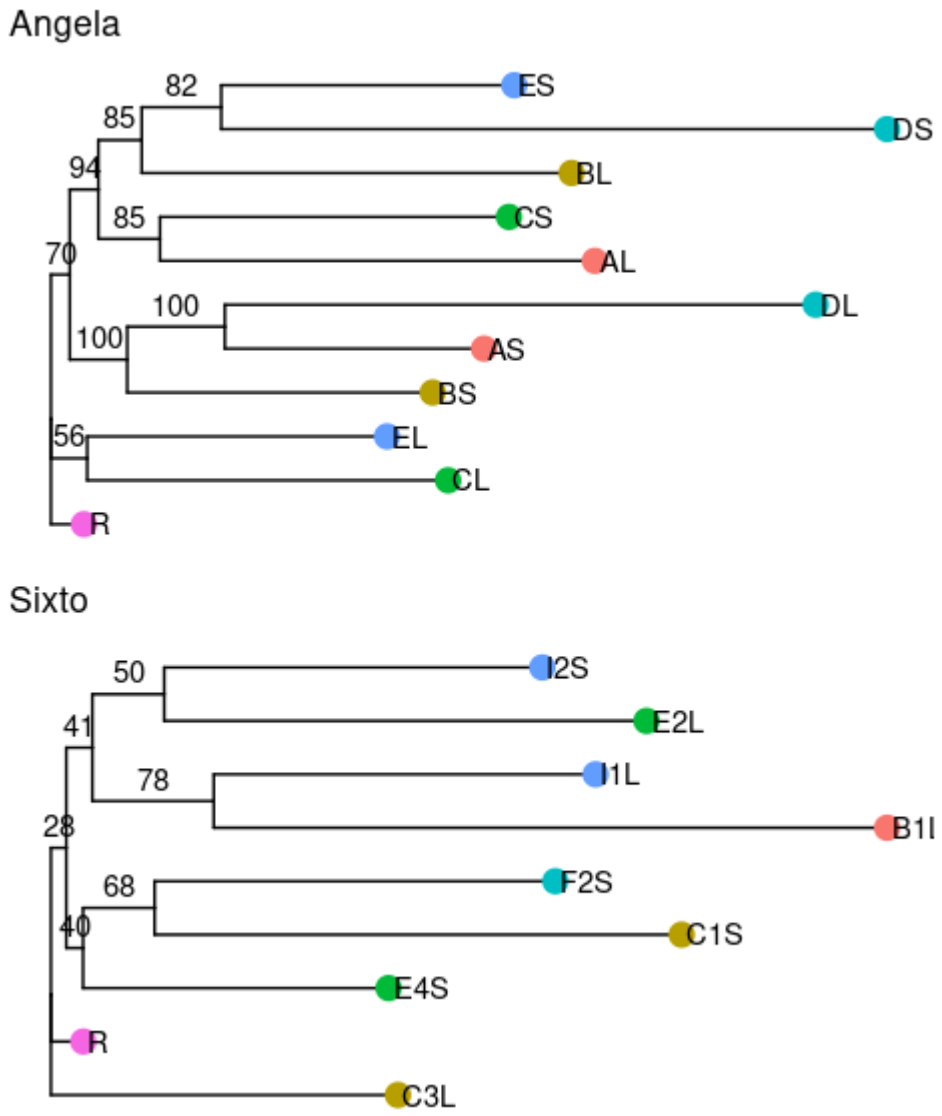

Figure F4: Phylogenies of the Angela and Sixto mutations. The phylogeny of the mutations was constructed with iqtree (Nguyen et al., 2015) with R defined as the root. Node labels indicate node confidence in percent assessed with 1000 bootstraps in iqtree.

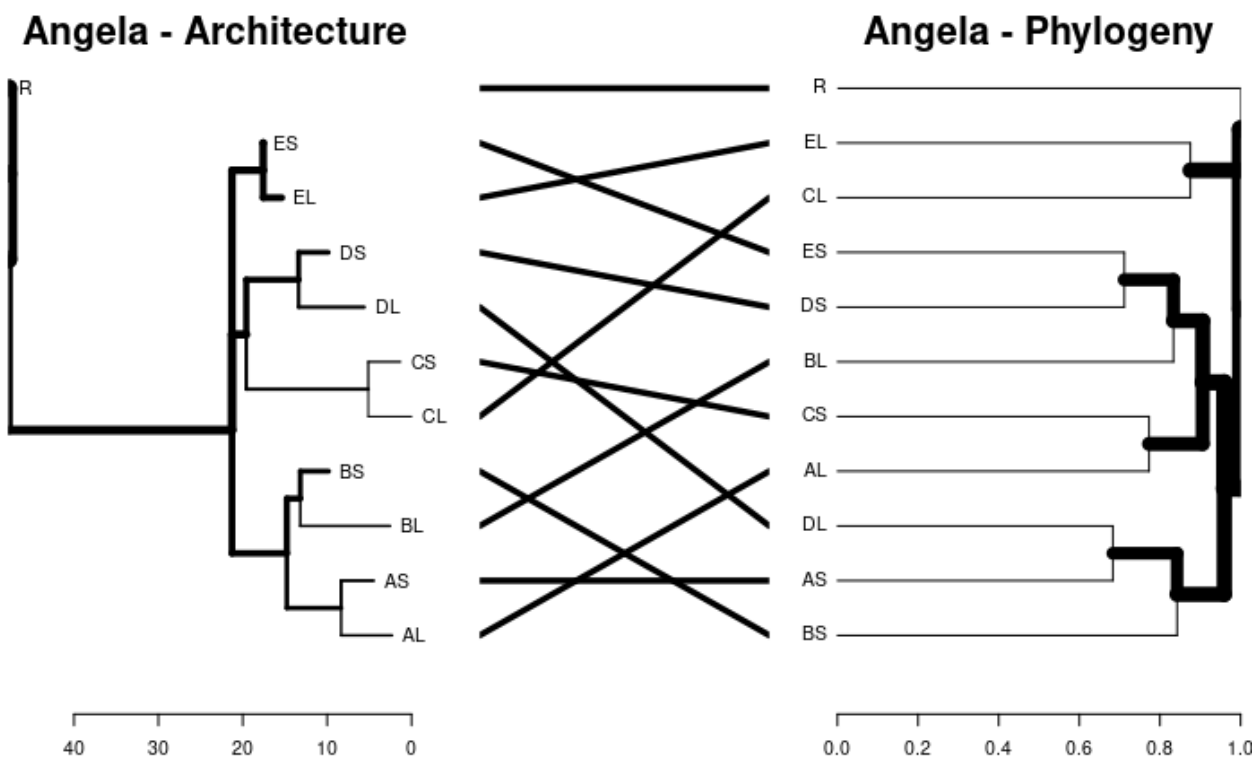

Figure F5: Comparison of the dendrograms of Angela's architecture with the phylogeny of Angela's mutations. X-axes represent distances in metres for the architecture and in substitution per base for the phylogeny.

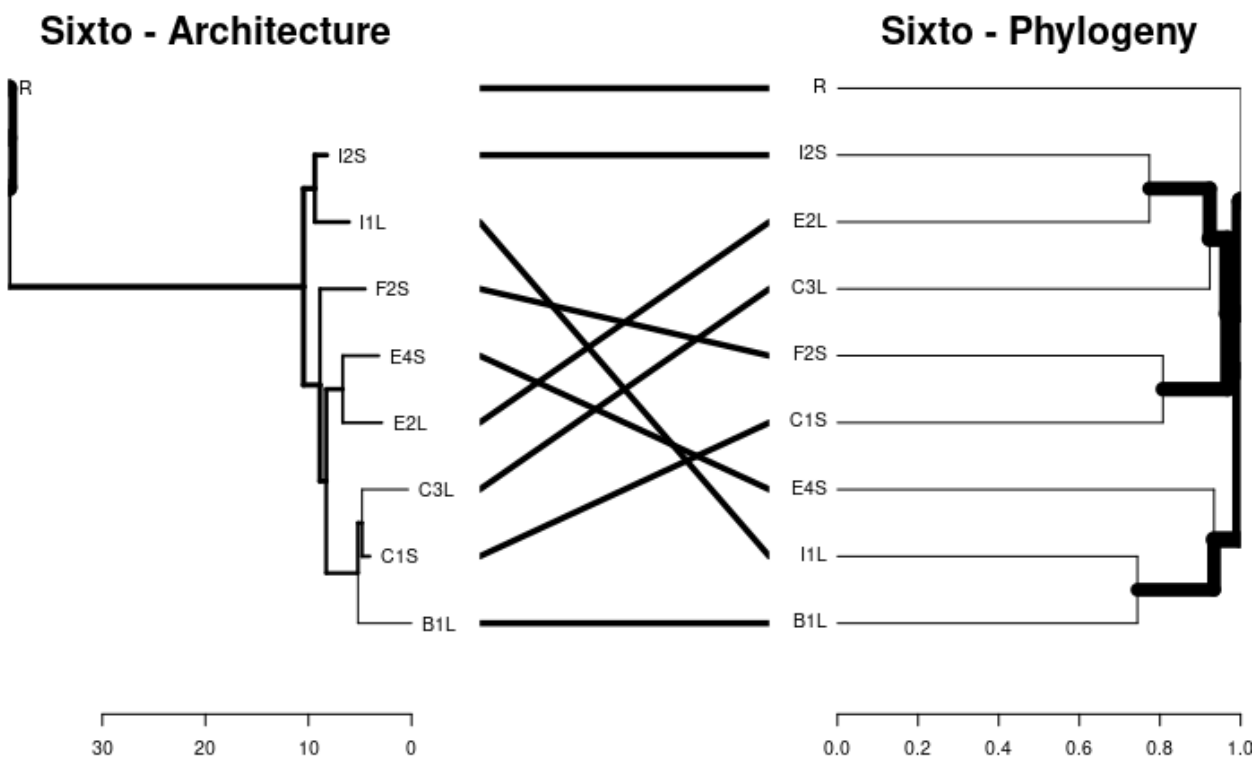

Figure F6: Comparison of the dendrograms of Sixto's architecture with the phylogeny of Sixto's mutations. X-axes represent distances in metres for the architecture and in substitution per base for the phylogeny.

G - Light and somatic mutations

We explored the effects of light on the occurrence of mutations in the trees using Student's T-tests and Kolmogorov-Smirnov tests. We compared the number of mutations detected in branches exposed to high vs. low light conditions using the leaves as an observation. Student's T-tests revealed no differences in the number of accumulated mutations between light and shadow conditions in both trees (Fig. G1), while Kolmogorov-Smirnov tests

revealed non-identical distributions between the two conditions (Fig. G2). We further compared mutation types (base change, Fig. G3) and mutation spectra (mutation context with 5' and 3' bases, Fig. G4 & Fig. G5) between high and low light conditions among branches of each tree. Student's T-tests again revealed no differences of mutation types and spectra between light and shadow conditions (Fig. G3, Fig. G4 & Fig. G5).

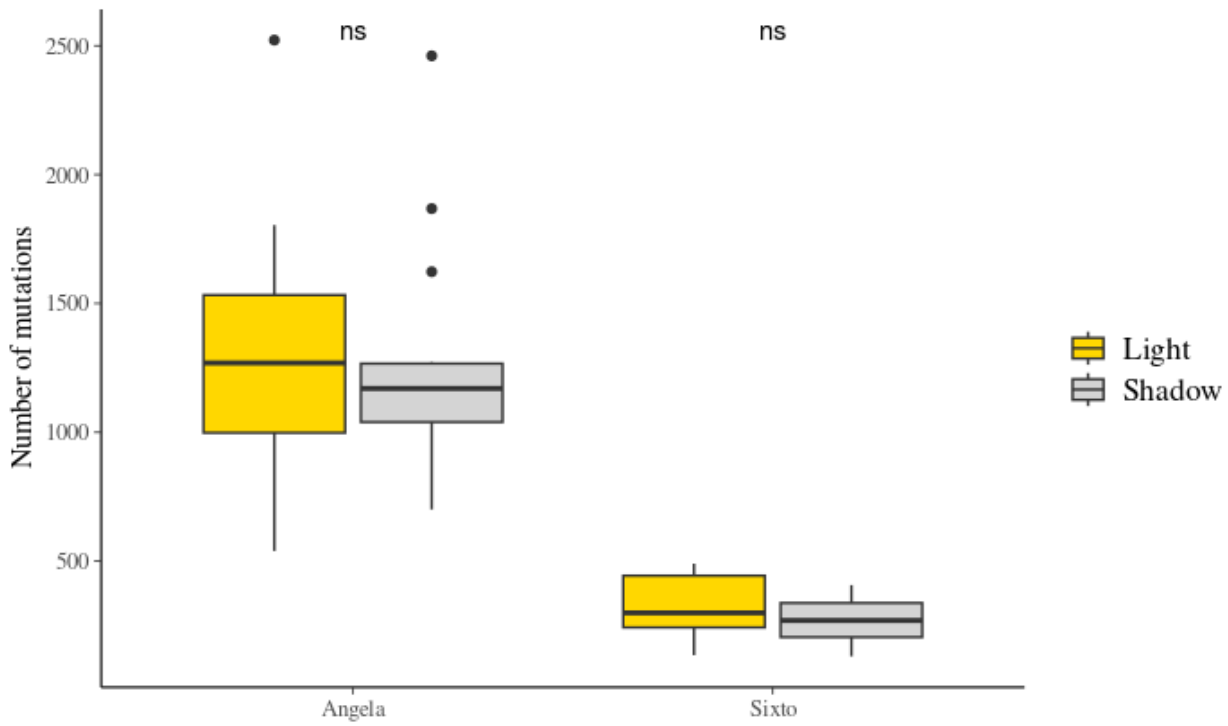

Figure G1: Effect of light exposure on somatic mutation accumulation in Angela and Sixto. Gold represents the number of mutations accumulated in leaves of the light-exposed branches and grey in leaves of the shaded branches. The "ns" labels indicate non-significant differences in the Student's T-tests.

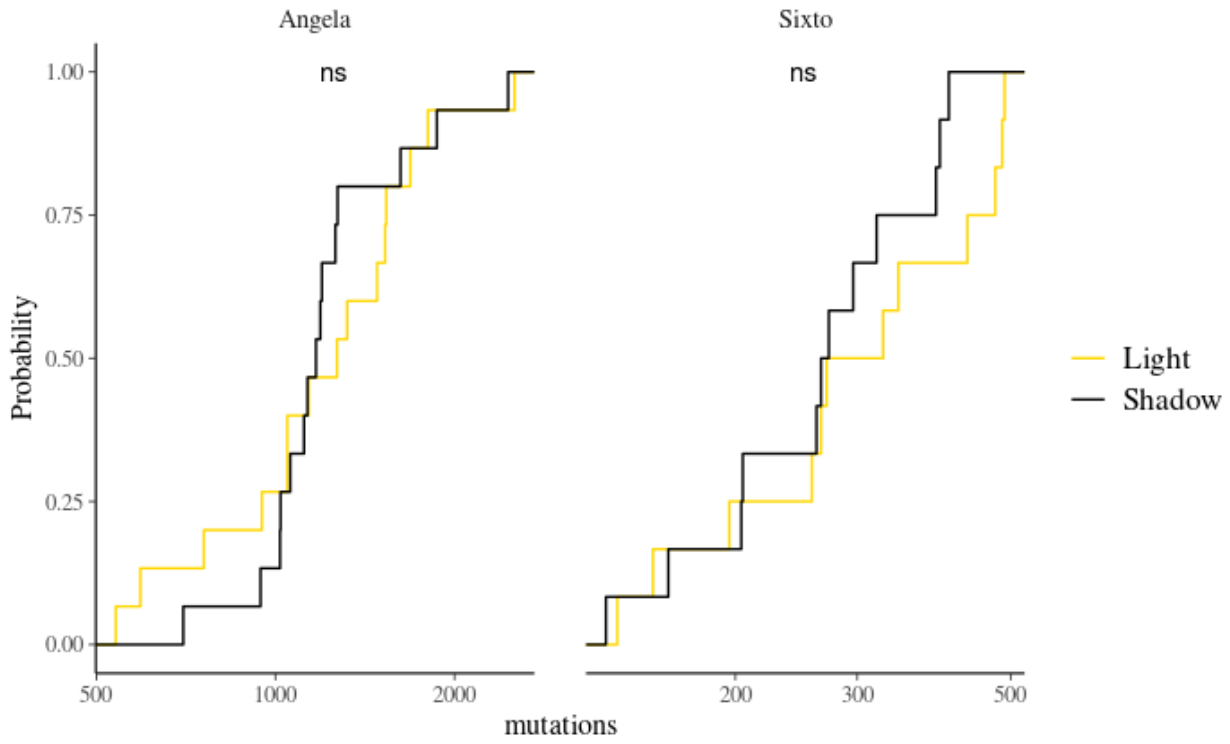

Figure G2: Empirical cumulative distribution of somatic mutations between leaves exposed to light and shade in Angela and Sixto. Gold represents the number of mutations accumulated in leaves of the light-exposed branches and black in leaves of the shaded branches. The "ns" labels indicate non-significant similarity in the Kolmogorov-Smirnov tests.

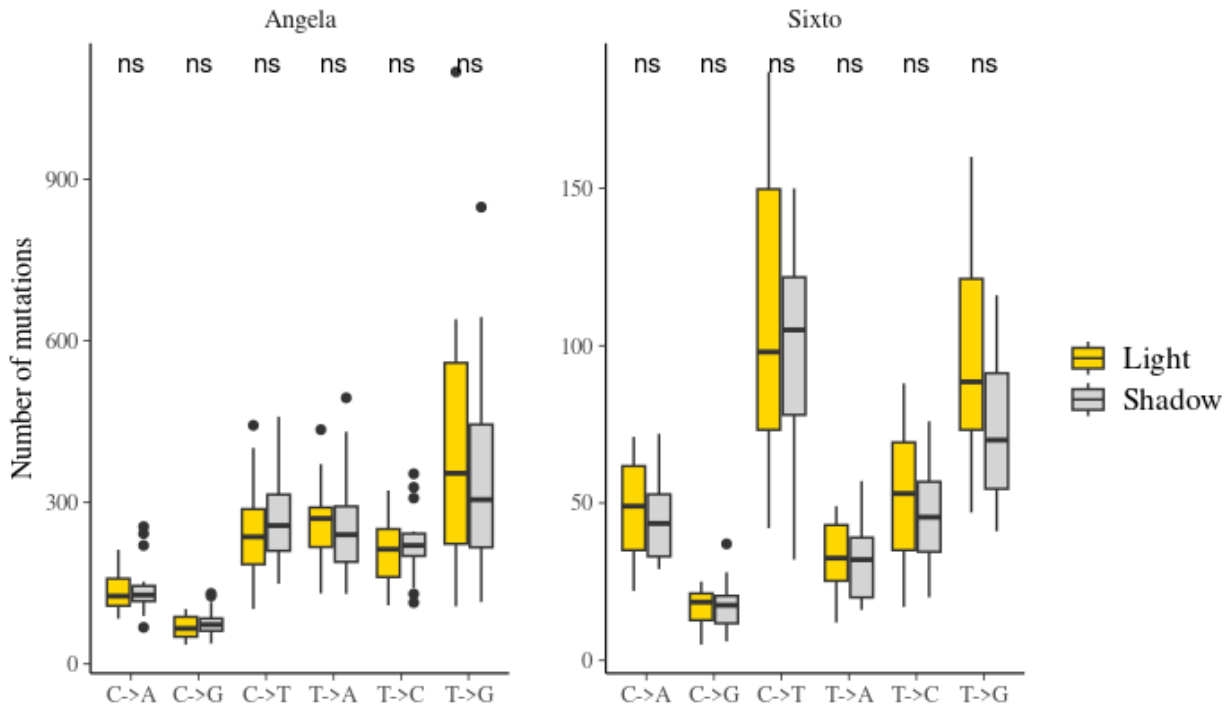

Figure G3: Effect of light exposure on somatic mutation accumulation in Angela and Sixto depending on mutation type. Gold represents the number of mutations accumulated in all leaves of the lighted tips and grey in all leaves of the shaded tips. The "ns" labels indicate non-significant differences in Student's T-tests.

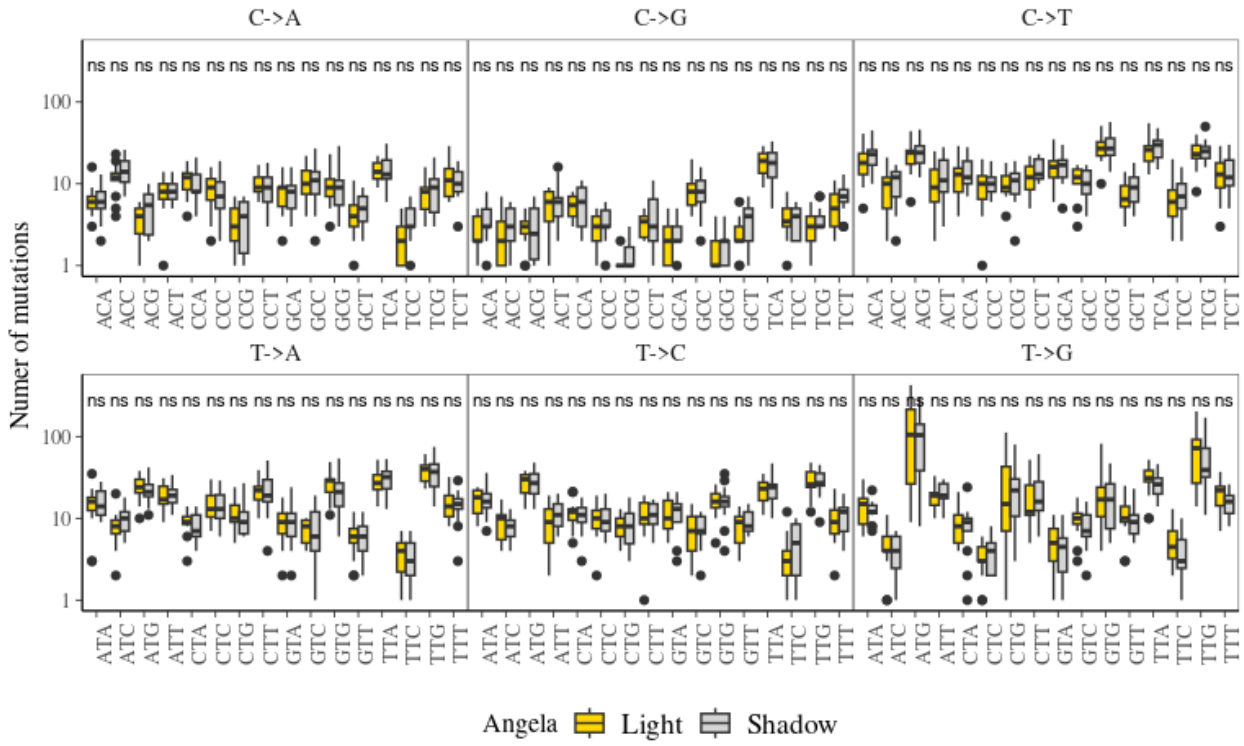

Figure G4: Effect of light exposure on somatic mutation accumulation in Angela depending on mutation spectra (mutation context with 5' and 3' bases). Gold represents the number of mutations accumulated in all leaves of the lighted tips and grey in all leaves of the shaded tips. The "ns" labels indicate non-significant differences in Student's T-tests.

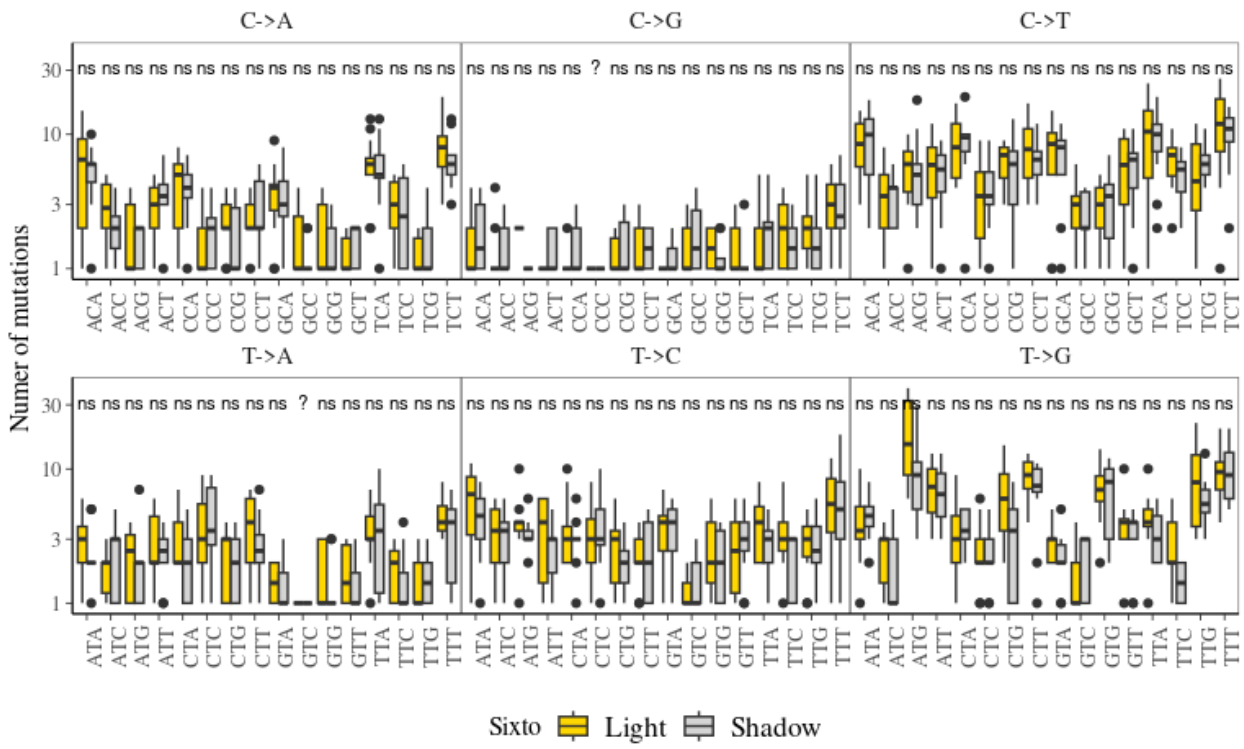

Figure G5: Effect of light exposure on somatic mutation accumulation in Sixto depending on mutation spectra (mutation context with 5' and 3' bases). Gold represents the number of mutations accumulated in all leaves of the light-exposed branches and grey in all leaves of the shaded branches. The "ns" labels indicate non-significant differences in Student's T-tests.

H - Low-frequency mutations

We explored the allelic fractions of somatic mutations in relation to tree sequencing depth (Fig. E1), a known determinant of the sensitivity of somatic mutation detection (Schmitt *et al.* 2022), for Sixto; Angela; two pedunculate oaks, *Quercus robur*, named Napoleon (Schmid-Siegert *et al.* 2017) and 3P (Plomion *et al.* 2018); and an unpublished dataset from

one tortuous beech *Fagus sylvatica* named Verzy (C. Plomion *pers. com.*). Most detected mutations were at low frequency (Fig. H1). The discrepancy in the number of observed mutations among sampled trees can be explained by an enrichment in low-fraction mutations in Angela (Fig. H1) detected thanks to the deeper sequencing (Fig. E1). For an allelic fraction above 0.25 (*i.e.,* medium-frequency to fixed mutations), we found the two tropical trees, Angela and Sixto, to have the lowest rate of somatic mutations, with 3 and 6 somatic mutations on 10 and 8 branches for Angela and Sixto, respectively, versus 56 to 421 somatic mutations on 2 to 3 branches for oak and beech (Fig. H1).

We further compared mutation annotations in terms of their presence in transposable elements (TE) and genes among trees. We assessed mutation functional impact using *SNPeff* (Cingolani *et al.,* 2012) and related non-synonymous mutations to their functional annotations, gene ontology, and allelic fraction. Focusing on coding regions, we detected 314 and 9 non-synonymous mutations and 567 and 31 synonymous mutations in Angela and in Sixto, respectively (Fig. H2). Gene ontology enrichment of genes associated to non-synonymous mutations was observed at genes coding for viral processes and in biotic interactions with other organisms in Angela (Fig. H3). Unfortunately, the 9 non-synonymous mutations in Sixto were not sufficient for similar analyses. We finally explored the allelic fraction of mutations depending on synonymy and found a significant negative effect ($p=1.47*10^{-14}$) of non-synonymy on the allelic fraction of mutations in both Angela and Sixto, indicating that novel non-synonymous mutations increase in allele frequency less frequently than synonymous ones, which suggests a potential overall negative intra-individual selection (Fig. H4).

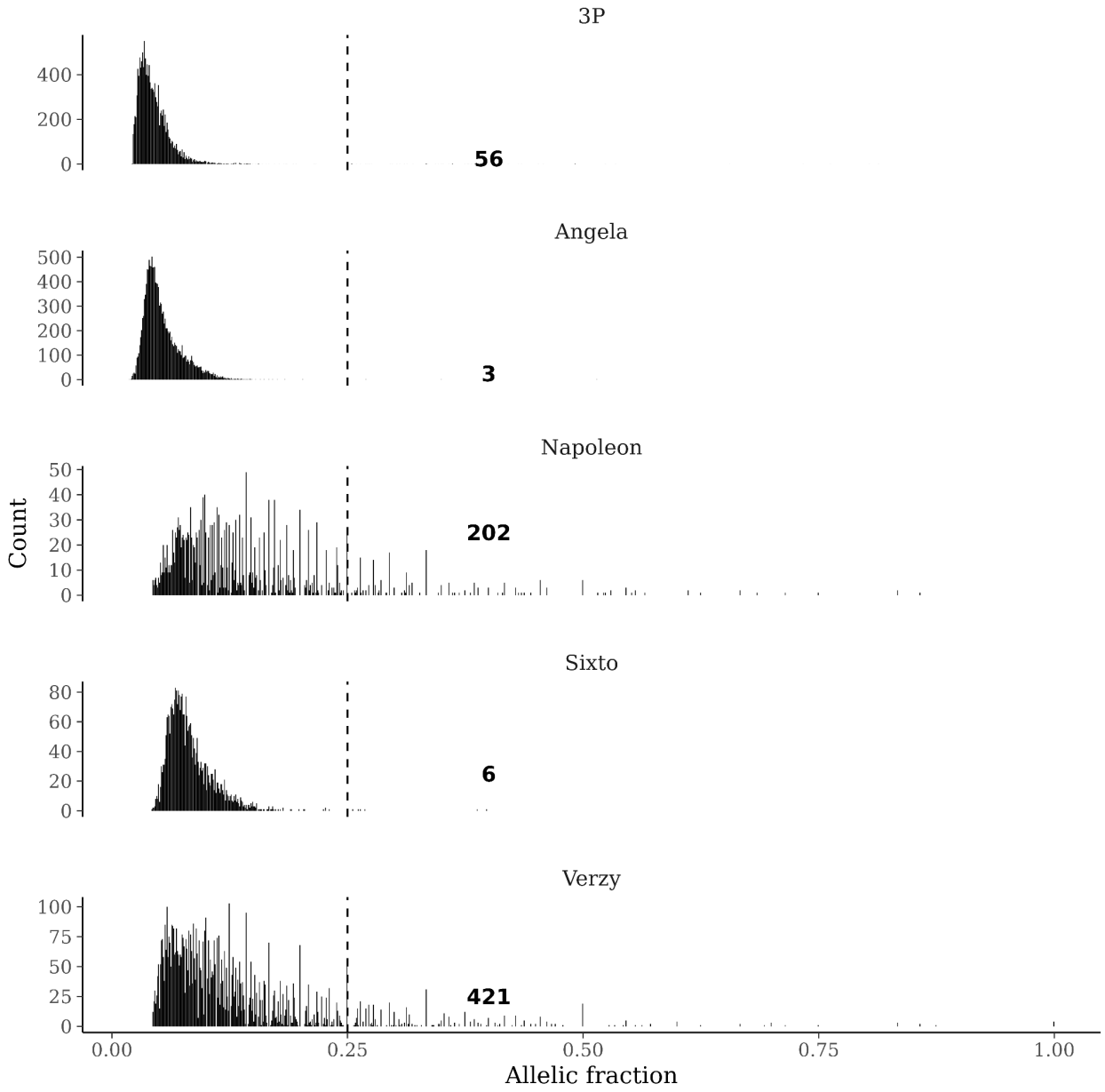

Figure H1: Distribution of allelic fractions for the Angela and Sixto mutations; for the two pedunculate oaks Quercus robur *reanalysed with the same pipeline: 3P and Napoleon (Schmitt et al., 2022); and an unpublished dataset from one tortuous beech* Fagus sylvatica *analysed with the same pipeline. The lower sequencing depth of Napoleon and Verzy explain their smaller left distribution.*

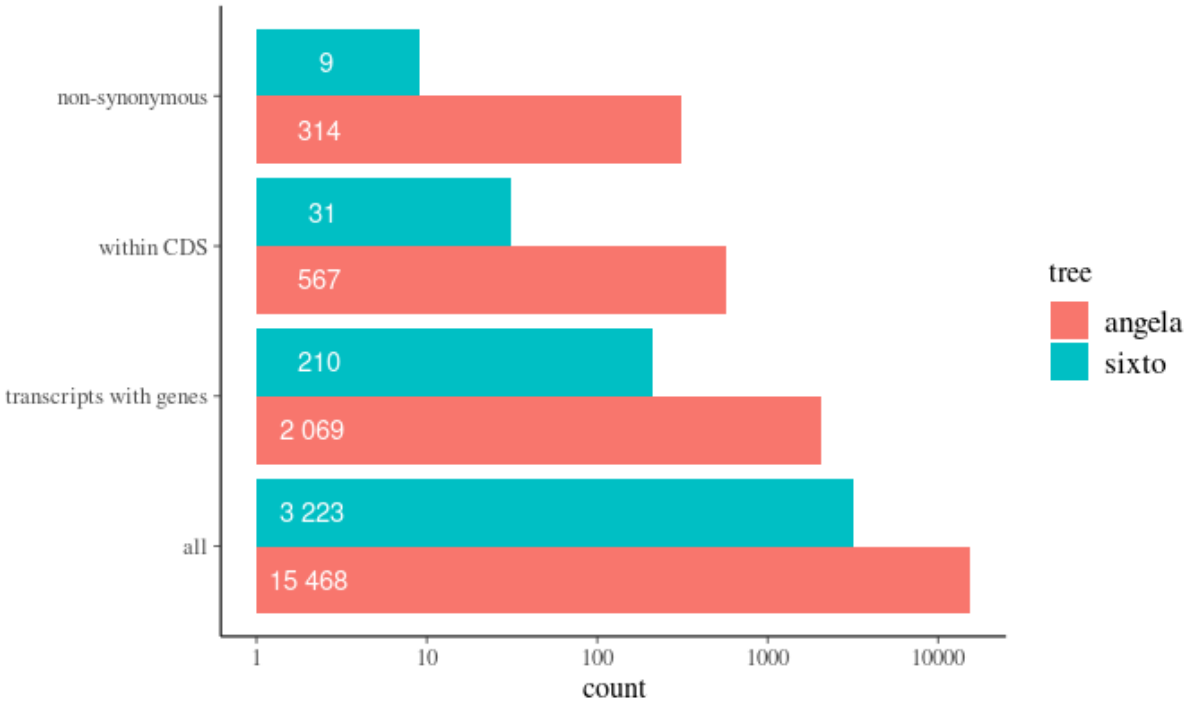

Figure H2: Mutation classified by functional impact with position and SNPeff (Cingolani et al., 2012) for Angela (red) and Sixto (blue). Mutations are classified into all, in a transcript with a coding DNA sequence, within the coding DNA sequence (CDS), and with at least one non-synonymous effect on the coding DNA sequences.

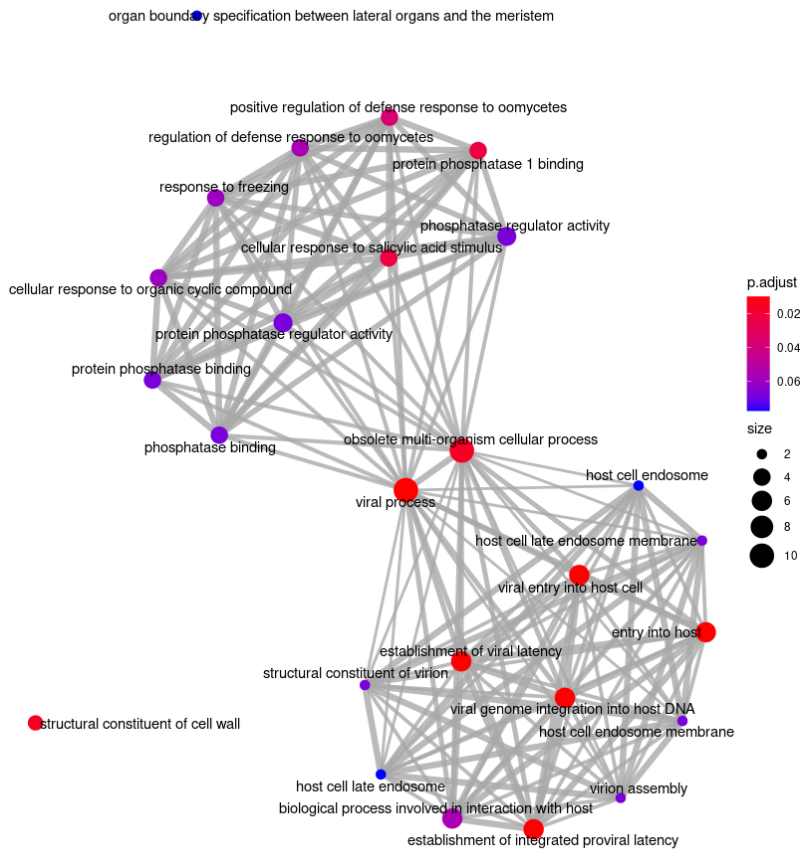

Figure H3: Enrichment map of the result of the over-representation of the enrichment analysis of gene sets with non-synonymous mutations in Angela. The enrichment in the ontology of genes carrying non-synonymous mutations was tested against all background gene ontologies. The colour represents the adjusted p-value and the size the number of connections to other enriched gene ontologies.

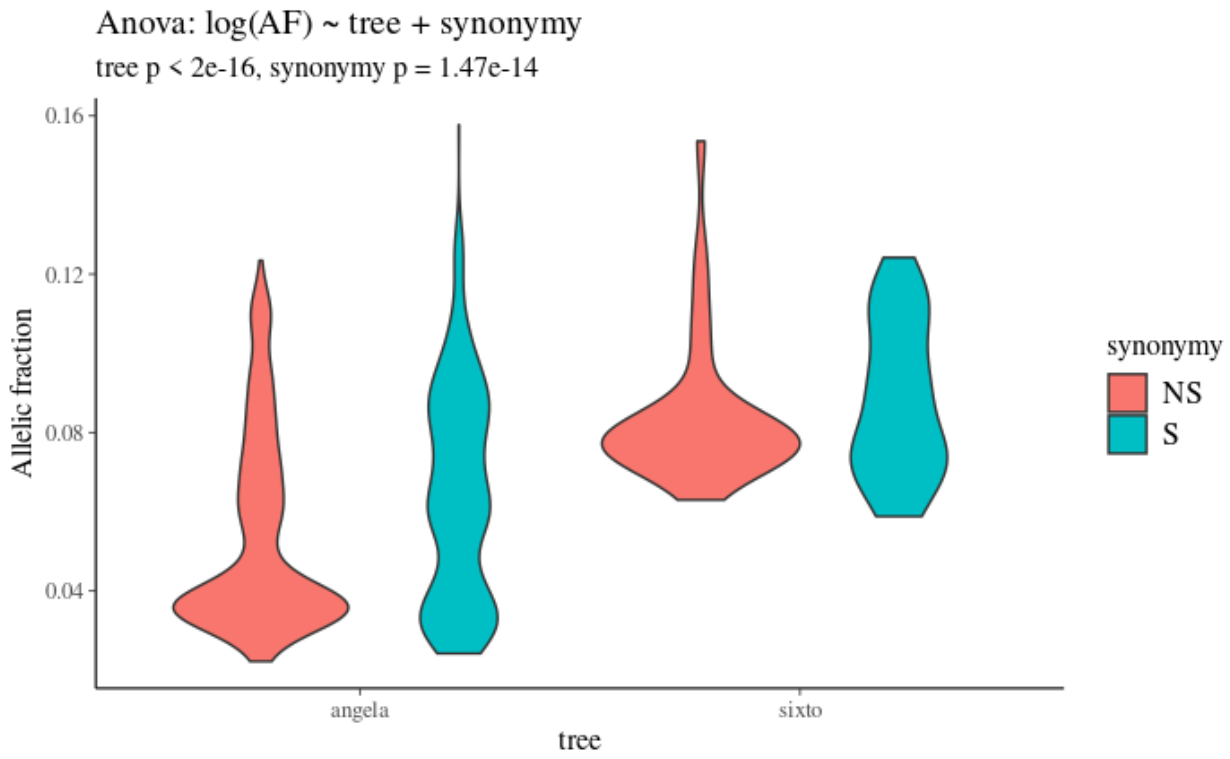

*Figure H4: Allelic fractions of synonymous (S, blue) and non-synonymous (NS, red) mutations for Angela and Sixto. Type II ANOVA testing differences in the log allelic fraction with tree and synonymy revealed a significant negative effect (p=1.47*10-14) of non-synonymy on the allelic fraction. The effect of trees is methodologically expected due to the greater sequencing depth in Angela allowing detection of lower allelic fractions.*

I - Fruit mutations redetections

We explored mutation transmission to fruit using amplicon resequencing. We kept as candidate mutations for redetection only mutations present in at least three leaves from the branches that had fruits during sampling for resequencing, which resulted in 160 candidate

mutations (124 for Angela and 36 for Sixto). Frozen fruits were dissected in 4 tissues: (i) embryo sac, (ii) nucellus, (iii) pericarp, and (iv) fruit base. Genomic DNA was extracted from 10-50 mg of frozen fruit tissue for both trees and additional leaf tissue for positive control with a CTAB protocol with chloroform - isoamyl alcohol (24:1) extraction, isopropanol precipitation and pellet resuspension in 1x Low TE (10 mM Tris-HCl + 0.1 mM EDTA; Doyle and Doyle 1987). DNA was quantified using a Qubit HS assay. Primer3plus (Untergasser et al., 2012) was used to design primer pairs targeting candidate mutations (amplicon size between 100 and 200 pb). Only one Angela candidate mutation failed to yield a primer pair. Illumina universal tags 5′-TCGTCGGCAGCGTCAGATGTGTATAAGAGACAG-3′ and 5′-GTCTCGTGGGCTCGGAGATGTGTATAAGAGACAG-3′ were added to the 5′ end of the forward and reverse primer sequences respectively. Oligonucleotides were ordered in a plate format from Integrated DNA Technologies with standard desalt purification at 25 nmoles synthesis scale. Each primer pair was tested using simplex PCR amplification of one DNA sample per species in a volume of 10 µL containing 2 µL of 5X Hot Firepol Blend master mix (Solis Biodyne), 1 µL of 2µM primer pairs, 1 µL of DNA (10 ng/µL), and 6 µL of PCR-grade water. We amplified the PCR on a Veriti 96-Well thermal cycler (Applied Biosystems) which consisted in an initial denaturation at 95°C for 15 min, followed by 35 cycles of denaturation at 95°C for 20 s, annealing at 59°C for 60 s, extension at 72°C for 30 s, and a final extension step at 72°C for 10 min. We checked the amplification on a 3% agarose gel. A total of six Angela primer pairs that failed to amplify were discarded at this stage. The remaining 101 Angela and 33 Sixto primer pairs, targeting respectively 117 and 36 mutations, were grouped accounting for potential primer dimer formation using Primer Pooler (Brown et al., 2017) for subsequent multiplex PCR amplification. Four multiplexed PCR were done for

each species in a volume of 10µL using 2 µL of 5X Hot Firepol Multiplex master mix (Solis Biodyne), 1 µL of multiplex primer mix (0.5 µM of each primer), 2 µL of DNA (10 ng/µL), and 5 µL of PCR-grade water. The amplification was done a Veriti 96-Well thermal cycler (Applied Biosystems) using an initial denaturation at 95°C for 12 min followed by 35 cycles of denaturation at 95°C for 30 s, annealing at 59°C for 180 s, extension at 72°C for 30 s, and a final extension step at 72°C for 10 min. The amplicons from the four multiplexed PCR of each sample were pooled. Illumina adapters and sample-specific Nextera XT index pairs were added to the amplicons by a PCR targeting the Illumina universal tags attached to the locus-specific primers. This indexing PCR was done in a volume of 20 µL using 5X Hot Firepol Multiplex master mix (Solis Biodyne), 5 µL of amplicon, and 0.5 µM of each of the forward and reverse adapters, using an initial denaturation at 95°C for 12 min followed by 15 cycles of denaturation at 95°C for 30 s, annealing at 59°C for 90 s, extension at 72°C for 30 s, and a final extension step at 72°C for 10 min. We then pooled the libraries and purified them with 0.9X Agencourt AMPure XP beads (Beckman Coulter, the UK). We checked the library quality on a Tapestation 4200 (Agilent) and quantified it using QIAseq Library Quant Assay kit (Qiagen, Hilden, Germany) in a Roche LightCycler 480 quantitative PCR. The libraries were sequenced on an Miseq sequencer (Illumina, San Diego, CA, USA) using a V2 flow cell with a 2x150 bp paired-end sequencing kit. We analysed the amplicon resequencing using *FDSTools* (Hoogenboom *et al.,* 2016) embedded into a pipeline used to format results, to compare blind-repeated genotyping to estimate genotyping error rate and to extract locus and allele information (Lepais *et al.,* 2020).

We further aligned consensus contigs of each haplotype on corresponding genomes with *BWA mem* (v0.7.17, Li & Durbin*,* 2009) and classified the status of mutations on each haplotype by manually examining the alignment on *IGV* (Thorvaldsdóttir *et al.,* 2013). We explored mutation transmission with strict detection and filtering of mutations in fruit tissues. We evaluated the transmission of somatic mutations with the highest stringency by removing: (1) suspect mutations based on genomic area inspection after consensus haplotypes alignments; (2) mutations inconsistent with branch origin; and (3), mutations inconsistent among fruit tissues. Mutations were classified as: (1) verified, *i.e.* identified in a realigned haplotype; (2) not redetected, *i.e.* corresponding haplotypes only had the reference allele; (3) unaligned, *i.e.* the amplicon did not cover the targeted genomic area; or (4) other cases, including mainly candidate mutations close to a poly-A repeat and one candidate mutation suspected to be a paralog. We found 21 verified mutations (15%) against 81 not redetected in the fruit (72%), but 21 did not align (15%) and 17 were suspicious (12%, Tab I1).

Among the 21 verified mutations, only 10 were present in embryos, the rest being present in maternal tissues (pericarp and fruit base) or positive controls composed by leaf tissues. We then focused on the 10 mutations transmitted to fruits embryos and further filtered by checking (1) the consistency between the origin of the mutation in the tree crown for the original leaves where it was detected with the origin of the fruit in the tree crown; and (2), the consistency between the fruit tissues, mainly whether the genotype of the cotyledon and embryo sac matched. We found most mutations in fruits from the same branch as their origin in the tree crown for the original leaves (Tab I2). Only 1 candidate transmitted

mutation to embryo (SNV057) showed mutations in fruits from boughs A and D while only detected in the leaves from bough B. However, as these mutations are low-frequency in the crown but fixed in the fruits, they could have been missed in the crown but found in the fruits. Finally, most mutations showed almost 100% consistency between the fruit tissues, *i.e.*, most genotypes of cotyledon and embryo sac matched (Tab I2). Only 1 candidate mutation transmitted to embryo (SNV057) showed 6 inconsistent fruits of the 52 samples (15%), but contamination during dissection due to the small size of the fruits could explain the inconsistencies.

In conclusion, even with the most stringent filtering, we validated the transmission of 10 mutations (6 in Angela and 4 in Sixto) from the tree crown to the fruits. Tree somatic mutations from the crown are thus transmitted to fruit embryos. Crown mutations were transmitted to 4 fruits of bough A, 5 fruits of bough B, 1 fruit of bough C and 2 fruits of bough D in Angela; whereas in Sixto, they were transmitted to only 4 fruits of bough B. (Fig. F1). The crown mutations transmitted to fruits included both recent mutations, originating from the BS and CL branches in Angela and the B1L branches in Sixto, and old mutations, originating from the base of the crown in Angela and the C and F intersections in Sixto (Tab I2). The crown mutations transmitted to fruits were all low-frequency mutations in their respective branch, with a mean allelic fraction from 0.038 to 0.088 (Tab I2).

We then explored the relationship between the rate of transmission of mutations to embryos and the median of the allelic fraction of mutation in leaves from their respective

branches and in the whole crown. We found a significant positive correlation (Pearson's r=0.65, p=0.011, Fig. I1), which supports a random transmission of mutations.

Table I1: Classification of candidate mutations redetected in fruits. Mutations were classified as: (1) ***verified:*** *identified in a realigned haplotype: (2)* ***not redetected:*** *corresponding haplotypes only had the reference allele: (3)* ***unaligned:*** *the amplicon was not covering the targeted genomic area; or (4),* ***other cases:*** *including mainly candidate mutations close to a poly-A repeat and one candidate mutation suspected to be a paralog.*

Mutation class	Angela	Sixto	Total	Percentage
Verified	16	5	21	15%
Not redetected	81	20	101	72%
Unaligned	16	5	21	15%
other cases	11	6	17	12%

Table I2: Mutations redetected in embryos of fruits across boughs. Columns indicate tree, mutation name, bough of origin of the mutation in the tree crown for the original leaves where it was detected, bough of origin of the fruit in the tree crown, number of embryos with the mutation, transmission rate to the embryos in percent, median of the allelic fraction of the mutations among leaves from the corresponding bough, percentage of match between genotypes of the cotyledon and embryo sac, and latest possible origin of the mutation in the crown of the tree based on the most recent branching event of the shared mutation by all samples carrying it. Bold lines of SNV057 indicate mismatch between genotypes of the cotyledon and embryo sac. Red lines of SNV057 indicate branches inconsistent with the bough of origin of the mutation in the tree crown for the original leaves where it was detected.

Tree	SNV	Bough origin	Bough fruit	Mutated embryos	Transmission rate (%)	Bough allelic fraction	Tissues match	Mutation origin
Angela	SNV006	A, B, C, D	A	5	25	0.042	100	X
Angela	SNV006	A, B, C, D	B	2	8	0.047	100	X
Angela	SNV013	A, B, C, D	A	1	5	0.05	100	X
Angela	SNV013	A, B, C, D	B	2	8	0.043	100	X
Angela	SNV031	A, B, D	B	1	4	0.054	100	X
Angela	SNV054	C	C	1	25	0.074	98	CL
Angela	**SNV057**	**B**	**A**	**5**	**25**		**85**	**BS**
Angela	**SNV057**	**B**	**B**	**4**	**16**	**0.074**	**85**	**BS**
Angela	**SNV057**	**B**	**D**	**1**	**17**		**85**	**BS**
Angela	SNV107	A, C, D	A	1	5	0.048	98	X
Angela	SNV107	A, B, C, D	B	4	16	0.031	98	X
Angela	SNV107	A, C, D	D	1	17	0.038	98	X
Sixto	SNV128	B, C, E, F	B	1	25	0.088	100	XF
Sixto	SNV132	B, C	B	1	25	0.067	100	XC
Sixto	SNV151	B	B	1	25	0.074	100	B1L
Sixto	SNV160	B	B	1	25	0.068	100	B1L

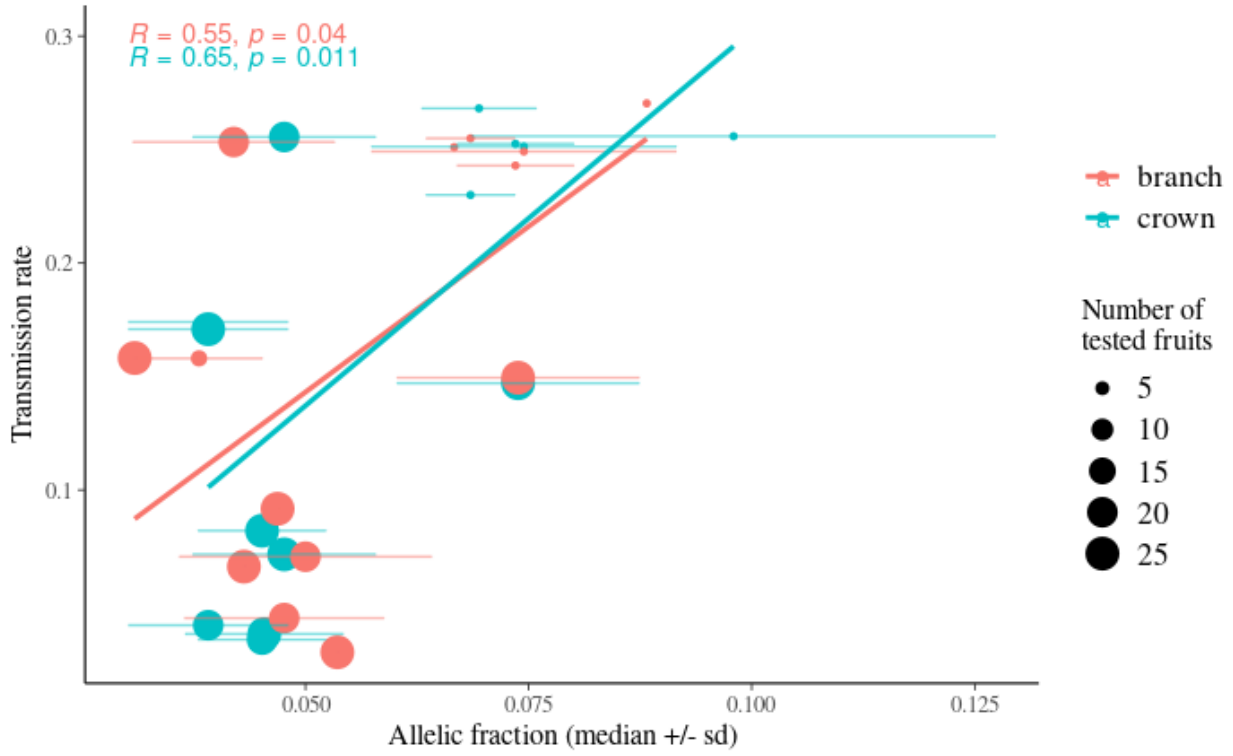

Figure I1: Relationship between the rate of transmission of mutations to embryos and the allelic fraction of the mutation transmitted in their respective boughs or in the whole crown. The blue dots represent the median in the whole crown while the red dots represent the median in their respective branches. The error bars represent the uncertainty of the allelic fraction with the median plus and minus the standard deviation. The size of the dots represents the total number of fruits tested, indicating the uncertainty of the transmission rate estimates. The red and blue lines represent the linear relationship between the two variables in the boughs or in the whole crown respectively. The text represents the Pearson correlation test with the value and the associated p-value.

J - Somatic mutations and population diversity

Any new mutation in the population appears at half the effective population size (Ne), regardless of whether the mutation is of germline or somatic origin, or whether it was initially at a low or high frequency. If the mutation is transmitted, the evolution of the allele frequency will depend mainly on the effects of drift. Consequently, the identification of new mutations requires the sequencing of families rather than populations, as it would take thousands or tens of thousands of generations for the mutation to increase in allele frequency in the population. Future studies could combine sequencing of families (e.g. trios) with the germline mutation rates in order to know which proportion of the mutation rates has a somatic origin.

References

Abrusán, G., Grundmann, N., Demester, L., & Makalowski, W. (2009). TEclass - A tool for automated classification of unknown eukaryotic transposable elements. *Bioinformatics*, *25*(10), 1329–1330. https://doi.org/10.1093/bioinformatics/btp084

Aguilos, M., Stahl, C., Burban, B., Hérault, B., Courtois, E., Coste, S., … Bonal, D. (2018). Interannual and Seasonal Variations in Ecosystem Transpiration and Water Use Efficiency in a Tropical Rainforest. *Forests*, *10*(1), 14. https://doi.org/10.3390/f10010014

Altschul, S. F., Gish, W., Miller, W., Myers, E. W., & Lipman, D. J. (1990). Basic local alignment search tool. *Journal of Molecular Biology*, *215*(3), 403–410. https://doi.org/10.1016/S0022-2836(05)80360-2

Auwera, G. A., Carneiro, M. O., Hartl, C., Poplin, R., del Angel, G., Levy-Moonshine, A., … DePristo, M. A. (2013). From FastQ Data to High-Confidence Variant Calls: The Genome Analysis Toolkit Best Practices Pipeline. *Current Protocols in Bioinformatics*, *43*(1), 483–492. https://doi.org/10.1002/0471250953.bi1110s43

Bateman, A., Martin, M. J., O'Donovan, C., Magrane, M., Apweiler, R., Alpi, E., … Zhang, J. (2015). UniProt: A hub for protein information. *Nucleic Acids Research*, *43*(D1), D204–D212. https://doi.org/10.1093/nar/gku989

Bolger, A. M., Lohse, M., & Usadel, B. (2014). Trimmomatic: A flexible trimmer for Illumina sequence data. *Bioinformatics*, *30*(15), 2114–2120. https://doi.org/10.1093/bioinformatics/btu170

Brůna, T., Hoff, K. J., Lomsadze, A., Stanke, M., & Borodovsky, M. (2021). BRAKER2: Automatic eukaryotic genome annotation with GeneMark-EP+ and AUGUSTUS supported by a protein database. *NAR Genomics and Bioinformatics*, *3*(1), 1–11. https://doi.org/10.1093/nargab/lqaa108

Brown, S. S., Chen, Y. W., Wang, M., Clipson, A., Ochoa, E., & Du, M. Q. (2017). PrimerPooler: automated primer pooling to prepare library for targeted sequencing. *Biology Methods and Protocols*, *2*(1), bpx006. https://doi.org/10.1093/biomethods/bpx006

Bryant, D. M., Johnson, K., DiTommaso, T., Tickle, T., Couger, M. B., Payzin-Dogru, D., … Whited, J. L. (2017). A Tissue-Mapped Axolotl De Novo Transcriptome Enables Identification of Limb Regeneration Factors. *Cell Reports*, *18*(3), 762–776. https://doi.org/10.1016/j.celrep.2016.12.063

Chen, Z. L., Meng, J. M., Cao, Y., Yin, J. L., Fang, R. Q., Fan, S. B., … He, S. M. (2019). A high-speed search engine pLink 2 with systematic evaluation for proteome-scale identification of cross-linked peptides. *Nature Communications*, *10*(1). https://doi.org/10.1038/s41467-019-11337-z

Cheng, H., Concepcion, G. T., Feng, X., Zhang, H., & Li, H. (2021). Haplotype-resolved de novo assembly using phased assembly graphs with hifiasm. *Nature Methods*, *18*(2), 170–175. https://doi.org/10.1038/s41592-020-01056-5

Cingolani, P., Platts, A., Wang, L. L., Coon, M., Nguyen, T., Wang, L., … Ruden, D. M. (2012). A program for annotating and predicting the effects of single nucleotide polymorphisms, SnpEff: SNPs in the genome of Drosophila melanogaster strain w1118; iso-2; iso-3. *Fly*, *6*(2), 80–92. https://doi.org/10.4161/fly.19695

Danecek, P., Bonfield, J. K., Liddle, J., Marshall, J., Ohan, V., Pollard, M. O., … Li, H. (2021). Twelve years of SAMtools and BCFtools. *GigaScience*, *10*(2), 1–4. https://doi.org/10.1093/gigascience/giab008

Detienne, P. (1995). Nature et périodicité des cernes dans quelques bois guyanais. *Bois et Forêts Des Tropiques*. Retrieved from http://cat.inist.fr/?aModele=afficheN&cpsidt=3454408

Doležel J., Greilhuber J., Lucretti S., Meister A., Lysák M.A., Nardi L., Obermayer R. (1998) Plant genome size estimation by fl ow cytometry: interlaboratory comparison. Annals of Botany 82 (Suppl. A): 17–26. https://doi.org/10.1093/oxfordjournals.aob.a010312

Doyle, J., & Doyle, J. (1987). Genomic plant DNA preparation from fresh tissue-CTAB method. *Phytochem Bull*, *19*(11), 11–15.

Drénou C (1988) Etude de l'architecture d'un arbre guyanais: l'angélique, dicorynia guianensis amshoff caesalpiniaceae. Master Thesis, Université de Montpellier II

Drénou C. 1994. Approche architecturale de la sénescence des arbres. Le cas de quelques angiospermes tempérées et tropicales. PhD thesis, University Montpellier 2.

Duan, Y., Yan, J., Zhu, Y., Zhang, C., Tao, X., Ji, H., … Wang, L. (2022). Limited accumulation of high-frequency somatic mutations in a 1,700-year-old Osmanthus fragrans tree . *Tree Physiology*, 1–10. https://doi.org/10.1093/treephys/tpac058

Finn, R. D., Clements, J., & Eddy, S. R. (2011). HMMER web server: Interactive sequence similarity searching. *Nucleic Acids Research*, *39*(SUPPL. 2), 29–37. https://doi.org/10.1093/nar/gkr367

Flynn, J. M., Hubley, R., Goubert, C., Rosen, J., Clark, A. G., Feschotte, C., & Smit, A. F. (2020). RepeatModeler2 for automated genomic discovery of transposable element families. *Proceedings of the National Academy of Sciences of the United States of America*, *117*(17), 9451–9457. https://doi.org/10.1073/pnas.1921046117

Galbraith D.W., Harkins K.R., Maddox J.M., Ayres N.M., Sharma D.P., Firoozabady E. (1983) Rapid flow cytometric analysis of the cell cycle in intact plant tissues., Science 220(4601): 1049–—1051. https://doi.org/10.1126/science.220.4601.1049

Galili, T. (2015). dendextend: An R package for visualizing, adjusting and comparing trees of hierarchical clustering. *Bioinformatics*, *31*(22), 3718–3720. https://doi.org/10.1093/bioinformatics/btv428

Heuertz, M., Caron, H., Scotti-Saintagne, C., Pétronelli, P., Engel, J., Tysklind, N., ... & Budde, K. B. (2020). The hyperdominant tropical tree Eschweilera coriacea (Lecythidaceae) shows higher genetic heterogeneity than sympatric Eschweilera species in French Guiana. Plant Ecology and Evolution, 153(1), 67-81.

Hoogenboom, J., van der Gaag, K. J., de Leeuw, R. H., Sijen, T., de Knijff, P., & Laros, J. F. J. (2017). FDSTools: A software package for analysis of massively parallel sequencing data with the ability to recognise and correct STR stutter and other PCR or sequencing noise. *Forensic Science International: Genetics*, *27*, 27–40. https://doi.org/10.1016/j.fsigen.2016.11.007

Kapitonov, V. V., & Jurka, J. (2008). A universal classification of eukaryotic transposable elements implemented in Repbase. *Nature Reviews Genetics*, *9*(5), 411–412. https://doi.org/10.1038/nrg2165-c1

Keller, R. (1994). Neglected vegetative characters in field identification at the supraspecific level in woody plants: phyllotaxy, serial buds, syllepsis and architecture. *Botanical Journal of the Linnean Society*, *116*(1), 33-51.

Köster, J., & Rahmann, S. (2012). Snakemake-a scalable bioinformatics workflow engine. *Bioinformatics*, *28*(19), 2520–2522. https://doi.org/10.1093/bioinformatics/bts480

Krogh, A., Larsson, B., Von Heijne, G., & Sonnhammer, E. L. L. (2001). Predicting transmembrane protein topology with a hidden Markov model: Application to

complete genomes. *Journal of Molecular Biology*, *305*(3), 567–580. https://doi.org/10.1006/jmbi.2000.4315

Kurtzer, G. M., Sochat, V., & Bauer, M. W. (2017). Singularity: Scientific containers for mobility of compute. *PLoS ONE*, *12*(5), 1–20. https://doi.org/10.1371/journal.pone.0177459

Lagesen, K., Hallin, P., Rødland, E. A., Stærfeldt, H. H., Rognes, T., & Ussery, D. W. (2007). RNAmmer: Consistent and rapid annotation of ribosomal RNA genes. *Nucleic Acids Research*, *35*(9), 3100–3108. https://doi.org/10.1093/nar/gkm160

Laurans, M., & Vincent, G. (2016). Are inter-and intraspecific variations of sapling crown traits consistent with a strategy promoting light capture in tropical moist forest?. *Annals of Botany*, *118*(5), 983-996.

Lepais, O., Chancerel, E., Boury, C., Salin, F., Manicki, A., Taillebois, L., … Guichoux, E. (2020). Fast sequence-based microsatellite genotyping development workflow. *PeerJ*, *2020*(3), 1–28. https://doi.org/10.7717/peerj.9085

Leitch IJ, Chase MW, Bennett MD. 1998. Phylogenetic analysis of DNA C-values provides evidence for a small ancestral genome size in flowering plants. Annals of Botany 82:85-94.

Li, H., & Durbin, R. (2009). Fast and accurate short read alignment with Burrows-Wheeler transform. *Bioinformatics*, *25*(14), 1754–1760. https://doi.org/10.1093/bioinformatics/btp324

Li, H., Handsaker, B., Wysoker, A., Fennell, T., Ruan, J., Homer, N., … Durbin, R. (2009). The Sequence Alignment/Map format and SAMtools. *Bioinformatics*, *25*(16), 2078–2079. https://doi.org/10.1093/bioinformatics/btp352

Loureiro J., Rodriguez E., Doležel J., Santos C. (2007) Two new nuclear isolation buffers for plant DNA flow cytometry: a test with 37 species. Annals of Botany 100(4): 875–888. https://doi.org/10.1093/aob/mcm152

Marçais, G., & Kingsford, C. (2011). A fast, lock-free approach for efficient parallel counting of occurrences of k-mers. *Bioinformatics*, *27*(6), 764–770. https://doi.org/10.1093/bioinformatics/btr011

Nguyen, L. T., Schmidt, H. A., Von Haeseler, A., & Minh, B. Q. (2015). IQ-TREE: A fast and effective stochastic algorithm for estimating maximum-likelihood phylogenies. *Molecular Biology and Evolution*, *32*(1), 268–274. https://doi.org/10.1093/molbev/msu300

Pedersen, B. S., & Quinlan, A. R. (2018). Mosdepth: Quick coverage calculation for genomes and exomes. *Bioinformatics*, *34*(5), 867–868. https://doi.org/10.1093/bioinformatics/btx699

Petersen, T. N., Brunak, S., Von Heijne, G., & Nielsen, H. (2011). SignalP 4.0: Discriminating signal peptides from transmembrane regions. *Nature Methods*, *8*(10), 785–786. https://doi.org/10.1038/nmeth.1701

Punta, M., Coggill, P. C., Eberhardt, R. Y., Mistry, J., Tate, J., Boursnell, C., … Finn, R. D. (2012). The Pfam protein families database. *Nucleic Acids Research*, *40*(D1), 290–301. https://doi.org/10.1093/nar/gkr1065

R Core Team. (2020). R: A Language and Environment for Statistical Computing. Vienna, Austria.

Schmitt, S., Leroy, T., Heuertz, M., & Tysklind, N. (2022). Somatic mutation detection: a critical evaluation through simulations and reanalyses in oaks. *Peer Community Journal*, *2*, e68. https://doi.org/10.24072/pcjournal.187

Seppey, M., Manni, M., & Zdobnov, E. M. (2019). BUSCO: Assessing Genome Assembly and Annotation Completeness. In *Notes on the Greek Text of Genesis* (Vol. 1962, pp. 227–245). https://doi.org/10.1007/978-1-4939-9173-0_14

Thorvaldsdóttir, H., Robinson, J. T., & Mesirov, J. P. (2013). Integrative Genomics Viewer (IGV): High-performance genomics data visualization and exploration. *Briefings in Bioinformatics*, *14*(2), 178–192. https://doi.org/10.1093/bib/bbs017

Untergasser, A., Cutcutache, I., Koressaar, T., Ye, J., Faircloth, B. C., Remm, M., & Rozen, S. G. (2012). Primer3—new capabilities and interfaces. *Nucleic acids research*, *40*(15), e115-e115. https://doi.org/10.1093/nar/gks596

Vester, H. F., & Cleef, A. M. (1998). Tree architecture and secondary tropical rain forest development: a case study in Araracuara, Colombian Amazonia. *Flora*, *193*(1), 75-97.

Vincent, G., Antin, C., Laurans, M., Heurtebize, J., Durrieu, S., Lavalley, C., & Dauzat, J. (2017). Mapping plant area index of tropical evergreen forest by airborne laser scanning. A cross-validation study using LAI2200 optical sensor. *Remote Sensing of Environment*, *198*, 254–266. https://doi.org/10.1016/j.rse.2017.05.034

Vurture, G. W., Sedlazeck, F. J., Nattestad, M., Underwood, C. J., Fang, H., Gurtowski, J., & Schatz, M. C. (2017). GenomeScope: Fast reference-free genome profiling from short reads. *Bioinformatics*, *33*(14), 2202–2204. https://doi.org/10.1093/bioinformatics/btx153